



# Climatic controls on biophysical interactions in the Black Sea under present day conditions and a potential future (A1B) climate scenario



Heather Cannaby<sup>a,b,\*</sup>, Bettina A. Fach<sup>b</sup>, Sinan S. Arkin<sup>b</sup>, Baris Salihoglu<sup>b</sup>

<sup>a</sup> National Oceanography Centre, Joseph Proudman Building, 6 Brownlow Street, Liverpool L3 5DA, United Kingdom

<sup>b</sup> Middle East Technical University, Institute of Marine Sciences, P.K. 28, 33731 Erdemli, Mersin, Turkey

## ARTICLE INFO

### Article history:

Received 28 August 2013

Received in revised form 24 July 2014

Accepted 6 August 2014

Available online 14 August 2014

### Keywords:

Black Sea

Modelling

Climatic Change

Biophysics

Primary Production

## ABSTRACT

A dynamical downscaling approach has been applied to investigate climatic controls on biophysical interactions and lower trophic level dynamics in the Black Sea. Simulations were performed under present day conditions (1980–1999) and a potential future (2080–2099) climate scenario, based on the Intergovernmental Panel for Climate Change A1B greenhouse gas emission scenario. Simulations project a 3.7 °C increase in SST, a 25% increase in the stability of the seasonal thermocline and a 37 day increase in the duration of seasonal stratification. Increased winter temperatures inhibited the formation of Cold Intermediate Layer (CIL) waters resulting in near complete erosion of the CIL, with implications for the ventilation of intermediate water masses and the subduction of riverine nutrients. A 4% increase in nitrate availability within the upper 30 m of the water column reflected an increase in the retention time of river water within the surface mixed-layer. Changes in thermohaline structure, combined with a 27% reduction in positive wind stress curl, forced a distinct change in the structure of the basin-scale circulation. The predominantly cyclonic circulation characteristic of contemporary conditions was reversed within the southern and eastern regions of the basin, where under A1B climatic conditions, anticyclonic circulation prevailed. The change in circulation structure significantly altered the horizontal advection and dispersion of high nutrient river waters originating on the NW shelf. Net primary production increased by 5% on average, with much spatial variability in the response, linked to advective processes. Phytoplankton biomass also increased by 5% and the higher nutrient environment of the future scenario caused a shift in species composition in favour of larger phytoplankton. No significant change in zooplankton biomass was projected. These results constitute one of many possible future scenarios for the Black Sea, being dependent on the modelling systems employed in addition to the choice of emission scenario. Our results emphasise in particular the sensitivity of dynamical downscaling studies to the regional wind forcing fields extracted from global models (these being typically model dependent). As atmospheric warming is projected with a high degree of confidence warming of the Black Sea upper layer, increased water column stability, and erosion of the CIL are believed to be robust results of this study.

© 2014 The Authors. Published by Elsevier B.V. This is an open access article under the CC BY-NC-ND license (<http://creativecommons.org/licenses/by-nc-nd/4.0/>).

## 1. Introduction

The recent work of Halpern et al. (2008, 2012) suggests that no area of the global ocean is unaffected by human influence, while a large fraction of the global ocean (41%) is strongly affected by multiple environmental stressors. As a consequence, marine ecosystems throughout the world are changing rapidly (Pauly et al., 1998). Mitigating and adapting to such change require an understanding of the cause and effect, i.e. an understanding of how ecosystems respond to perturbations in individual drivers of change. When a system is exposed to multiple

environmental stressors, isolating the response to an individual perturbation in forcing is often difficult, however, due to the existence of non-linearities and feedbacks within the system. Coupled ocean-ecosystem models are one of the few tools available which can be used to assess marine ecosystem sensitivity to individual changes in environmental drivers as well as to multiple environmental pressures applied synergistically. The Atmosphere Ocean General Circulation Models (AOGCMs) used to generate global scale projections for the Intergovernmental Panel on Climate Change Assessment Report Four (IPCC AR4, 2007; Meehl et al., 2007) are generally on too coarse a grid scale to be relevant to regional seas (e.g. Allen et al., 2010; Penduff et al., 2010). Furthermore, semi-enclosed seas such as the Black Sea are typically either excluded from or poorly represented by AOGCMs because exchanges through the narrow straits linking these seas with open water cannot be appropriately represented by the coarse grid resolution of the global

\* Corresponding author at: National Oceanography Centre, Joseph Proudman Building, 6 Brownlow Street, Liverpool L3 5DA, United Kingdom. Tel.: +90 44 151 7954957.

E-mail addresses: [heanna@noc.ac.uk](mailto:heanna@noc.ac.uk) (H. Cannaby), [bfach@ims.metu.edu.tr](mailto:bfach@ims.metu.edu.tr) (B.A. Fach), [sinan.arkin@ims.metu.edu.tr](mailto:sinan.arkin@ims.metu.edu.tr) (S.S. Arkin), [baris@ims.metu.edu.tr](mailto:baris@ims.metu.edu.tr) (B. Salihoglu).

models. The assessment of climate change impacts on marine ecosystems at the regional level, therefore, requires a downscaling approach.

This paper describes the application of a dynamical downscaling approach to assess the biophysical responses of the Black Sea to anthropogenically induced climate change. Climate change modulates primary production in marine systems through three main mechanisms: (i) direct physiological responses to a changing environment (e.g. temperature controls on phytoplankton growth rates), (ii) water column stability and processes of vertical transport (which mediate nutrient re-supply from below the euphotic zone and the exposure of phytoplankton to light) and, (iii) advective process which distribute high nutrient water masses such as arising from river plumes (Holt et al., 2014). The following paragraphs summarise how the physical characteristics of the Black Sea influence nutrient distribution and primary production in this basin.

The Black Sea is a highly stratified basin, characterised by a thin relatively fresh surface layer of riverine origin, overlaying saline waters of Mediterranean origin. Due to the strong stratification, MLDs are shallow, ranging from ~5 m in summer to between ~70 and 140 m depth in winter. A permanent halocline at 150–200 m depth prevents deep winter convection. Cool surface waters formed during winter penetrate to the depth of the upper halocline, forming a Cold Intermediate Layer (CIL), which typically persists throughout the year and is defined at its upper and lower boundaries by the 8 °C isotherm (Ivanov et al., 1997; Ozsoy and Unluata, 1997). The lower boundary of the CIL ranges from 40 m depth in cyclonic regions to 160 m depth in anticyclonic regions. CIL formation is thought to be concentrated in the central regions of the Black Sea basin and on the NW shelf, although the relative contribution of these two sources is still debated. Stanev et al. (2003) suggested that 60% of the CIL water mass may originate on the NW shelf, while more recent studies have suggested that NW shelf waters contribute 16–25% of the CIL volume (Mikaelyan et al., 2013 and references therein). Tugrul and Salihoglu (2003) suggested that CIL formation on the NW shelf plays an important role in the subduction of nutrient rich shelf waters into the upper pycnocline, thus removing nutrients from the euphotic zone. McQuatters-Gollop et al. (2008) suggest that this process modulates interannual variability in production, such that exceptionally warm years when CIL formation is considerably reduced are associated with anomalously high nutrient concentrations in the euphotic zone.

The large scale circulation of the Black Sea is dominated by a basin wide cyclonic gyre, with a narrow intense rim current associated with the shelf edge. A number of smaller quasi-permanent, anti-cyclonic eddies, including the prominent Batumi eddy in the southeast, are distributed between the rim current and the coast. The cyclonic circulation is predominantly driven by wind stress curl and modulated by the seasonal evolution of heat and freshwater fluxes (Korotaev et al., 2001; Ozsoy and Unluata, 1997; Stanev, 1990). Positive wind stress curl results in frictional convergence, driving Ekman pumping and upwelling of the pycnocline in the centre of the basin and depression of the pycnocline in coastal regions. The resultant sea surface slope which is most intense near the shelf edge drives a geostrophic current which approximately follows the 200 m contour, forming a rim current, which has an average width of 50 km (Ozsoy and Unluata, 1997).

The Black Sea is anoxic below the permanent pycnocline, meaning all aerobic life is confined to the upper ~200 m of the basin. The shallow anoxic interface results in unique processes of biogeochemical cycling, modulated by the downward flux of organic matter, and the existence of the permanent pycnocline which restricts vertical mixing. Under oxic conditions organic matter is oxidised and organic nitrogen is ultimately converted to nitrate. Under suboxic and anoxic conditions nitrate and nitrite are consumed by denitrification and anammox processes. As a result nitrate peaks below the euphotic zone at  $\sigma_t \sim 15.5$  and disappears at the anoxic interface (Murray et al., 2003). In open water regions of the Black Sea, nutrient supply is dominated by vertical fluxes driven by wind mixing and vertical convection, with winter

convection believed to be the dominant process (Oguz et al., 2008). Hence, phytoplankton seasonality is closely linked to water column stability and Mixed Layer Depth (MLD). Nezhlin et al. (2002) suggest that away from the NW shelf, the highly stratified nature of the Black Sea results in a seasonal cycle of phytoplankton biomass which is more akin to that typical of subtropical regions (e.g. as described by Longhurst, 1995). During a typical year phytoplankton biomass peaks during September and October and remains high throughout the winter months, decreasing during spring due to the onset of seasonal stratification (McQuatters-Gollop et al., 2008; Nezhlin, 2008; Nezhlin et al., 2002). Nezhlin et al. (2002) explain this seasonality by suggesting that processes which decrease stratification (wind mixing and convective mixing) enhance productivity. As production in the Black Sea continues throughout the winter months, nutrients do not accumulate within the mixed layer to the extent observed in temperate systems. With the onset of stratification in spring, the vertical resupply of nutrients is halted and production within the surface mixed-layer begins to decline. There is no evidence for the existence of a spring bloom in the Black Sea except at localised coastal stations (Kopelevich et al., 2002; Nezhlin et al., 2002). Seasonality, however, explains only 35% of variance in the chlorophyll-a time series (Vantrepotte and Melin, 2009). Warmer years such as 2001 have been characterised by higher than average biomass throughout the year and differed from the mean trend in the existence of distinct spring and autumn blooms. Hence there is evidence of a strong temperature control on phytoplankton seasonality in the Black Sea (McQuatters-Gollop et al., 2008; Oguz et al., 2003), although whether this is the result of top-down or bottom-up control remains a matter of discussion (e.g. Oguz et al., 2003).

The NW shelf and adjacent regions of the Black Sea are strongly influenced by riverine inputs from the Danube which discharges ~202 km<sup>3</sup> yr<sup>-1</sup>, and from the Dniester and Dnieper which together discharge ~50 km<sup>3</sup> yr<sup>-1</sup> (Ludwig et al., 2010). These rivers are highly eutrophic. Nitrate concentration at the Danube outflow was reported to average 232 µM between 1989 and 1993, and 178 µM between 1994 and 1995 (Lancelota et al., 2002). The distribution of high nutrient river water through advective processes forms a dominant control on the supply of nutrients to the NW shelf over both seasonal and inter-annual timescales. As a consequence, peak phytoplankton biomass is observed on the NW shelf during May and June, following peak river discharges during April and May (McQuatters-Gollop et al., 2008; Mikaelyan et al., 2013; Nezhlin, 2008).

The Black Sea is a highly impacted basin, subjected to a multitude of human induced environmental pressures in addition to climate change. These include eutrophication, overfishing, pollution, damming of rivers, and the introduction of alien species (e.g. BSC, 2008; Oguz and Velikova, 2010). Each of these environmental pressures has directly contributed to the degradation of the Black Sea environment, and as a result the ecosystem of the Black Sea has undergone dramatic changes since the early 1970s. Ecosystems such as the Black Sea which are already highly impacted may be particularly sensitive to climate change (e.g. Doney et al., 2012). Hence it is particularly important to consider the potential implications of climate change when developing management strategies for the Black Sea.

## 2. Experimental design

### 2.1. Study area

The Black Sea is an inland sea located between 41°–46°N and 28°–42°E, connected to the Sea of Marmara via the Bosphorus Strait and the Azov Sea via the Kerch Strait. The shelf edge slope is steep and the shelf is generally narrow except in the north-western shelf region (Fig. 1). The average depth of the north-western shelf, which comprises nearly 20% of the total basin area, is ~50 m (Oguz et al., 2005). The Black Sea drains a catchment area of 2 million km<sup>2</sup> and receives waste water from 100 million people (Mee, 1992), more than half of which enters

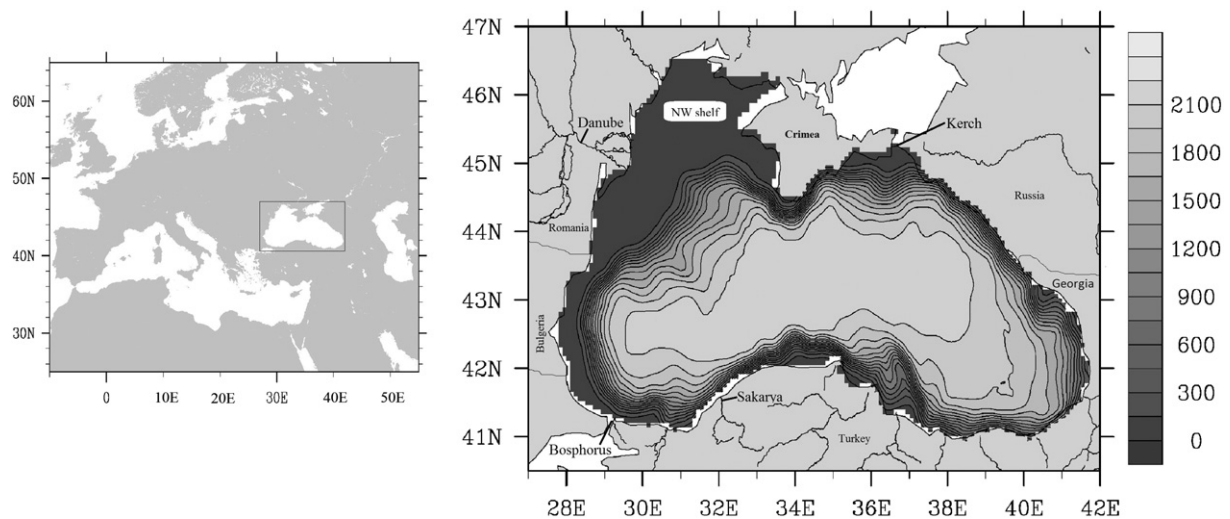


Fig. 1. Geographic location of the Black Sea (left) and Black Sea bathymetry (right).

the Black Sea via the NW shelf. The total fresh water budget into the Black Sea amounts to  $\sim 550 \text{ km}^3 \text{ yr}^{-1}$ . The positive water budget of the Black Sea is balanced by a net outflow through the Bosphorus, while the salt budget is conserved by the difference in salinities of the inflowing and outflowing water. Exchange through the Bosphorus can be described as a two-layered flow with an upper-layer outflow amounting to  $\sim 600 \text{ km}^3 \text{ yr}^{-1}$  with salinities within the range 16–18, and a lower layer influx of  $\sim 300 \text{ km}^3 \text{ yr}^{-1}$  with salinities in the range 35–37.5 (Ozsoy et al., 1986; Ozsoy et al., 1988).

## 2.2. Scenario definition

Three factors must be considered when defining the forcing fields for regional climate simulations, the choice of AOGCM(s) used to force the regional model, the emission scenario(s) and the time frame over which future simulations will be conducted. For both AOGCM and emission scenario definition, this study utilised the Coupled Model Intercomparison Project (CMIP) activities which informed the Intergovernmental Panel on Climate Change (IPCC) assessment reports. The IPSL-CM4-V2 climate model (Marti et al., 2006) was chosen because high frequency forcing was readily available. This study utilised the IPSL-CM4-V2 simulation member identified as LU20C2. The emission scenario assumed here is the Special Report on Emissions Scenarios (SRES) A1B socio-economic ‘story line’. The A1 storyline and scenario family describe a future world of very rapid economic growth, global population that peaks in mid-century and declines thereafter, and the rapid introduction of new and more efficient technologies. The A1B scenario assumes a balance between the use of fossil fuels and alternative energy sources. Within the range of SRES story lines A1B represents a moderate increase in atmospheric  $\text{CO}_2$  concentrations (850 ppm of  $\text{CO}_2$ -eq concentrations in 2100, where  $\text{CO}_2$ -eq describes the concentration of  $\text{CO}_2$  which would cause the equivalent increase in radiative forcing as would be obtained by summing all greenhouse gasses).

Climate impact studies require looking far enough into the future to ensure that the climate change signal can be resolved above the underlying climate variability. Rather than conducting a full transient simulation, we assume a time slice approach in which the statistics of a future period are compared with a present day control run. This approach requires that statistics within the time slice should be approximately stationary, requiring a minimum time slice window of 20 years. This paper compares the mean characteristics of a 20 year Present Day (PD) simulation extending from 1980 to 2000 to a 20 year future simulation extending from 2080 to 2100 (hereinafter referred to as A1B). A

Hind Cast (HC) reference simulation extending from 1980 to 2000 was also conducted, allowing model comparison with contemporary observations (since the AOGCM forced simulation could only be validated in a statistical sense). Atmospheric forcing for the HC reference simulation was obtained from the ECMWF ERA40 reanalysis (Uppala et al., 2005).

## 2.3. Description of models

The hydrodynamic model applied in this study was the Princeton Ocean Model (POM) using the Mellor–Yamada level 2.5 turbulence parameterisation (Blumberg and Mellor, 1987). The model domain which encompassed the entire Black Sea (41°S–46°N, 28°E–41.5°E), although excluding the Azov Sea, consisted of a  $7 \text{ km} \times 8 \text{ km}$  resolution, Arakawa C horizontal grid and a 26 level, sigma-coordinate vertical grid. The sigma-levels were compressed towards the surface and bottom. The maximum depth of the model domain was 2200 m. Because the Black Sea is a semi-enclosed basin, the lateral boundary conditions were no-slip and zero heat flux and salt fluxes everywhere except at the mouths of the Bosphorus and Kerch straits, and the 8 largest rivers surrounding the Black Sea (Danube, Dniester, Dnieper, Inguri, Rioni, Yesilirmak, Kizilirmak and Sakarya). At the mouths of the rivers and straits, temperature and salinity boundary conditions were specified as inflow conditions. Diffusive heat and salt fluxes were set to zero in the straits outflow points. Surface atmospheric forcing was prescribed using 6-hourly fields of wind stress, fresh water fluxes (evaporation, convective precipitation and large-scale precipitation), and heat flux fields (surface shortwave radiation, surface long-wave radiation, evaporative heat flux, and sensible heat flux). Temperature and salinity initial conditions for HC and PD simulations were defined using monthly mean climatologies for January from the World Ocean Atlas 2009 (Antonov et al., 2010; Locarnini et al., 2010). The IPSL-CM4 model output did not capture the permanent pycnocline of the Black Sea and therefore could not be used to generate initial conditions for the downscaled hydrodynamic model. Rather, the A1B simulation was spun up from present-day climatological data. All time slice simulations were spun up from rest over a period of 25 years, repeating on a cyclical basis the first year of the simulation. A 25 year spin-up was found to be sufficient to allow the seasonal cycle in SST to reach a steady state. Exchanges through the Danube and Kerch Straits and inflows from the rivers were defined by monthly mean volume flux, temperature and salinity climatologies. Nitrate input from rivers was defined as monthly mean time series for the HC and PD simulations and as monthly mean climatologies (calculated by averaging the 1980–1999 data set) for the A1B

simulation. The river data used in this study was collated within the framework of the EU sixth framework programme, SESAME (Ludwig et al., 2009, 2010). Riverine inputs of ammonia were parameterised as 33% of the nitrate input. For the future simulation the volume flux of river water entering the basin was scaled by the difference in precipitation between the PD and A1B simulation periods (following Holt et al., 2011). The freshwater balance was maintained throughout each simulation by artificially adjusting the volume of the outflow through the Bosphorus and the salinity of the Mediterranean waters entering the basin.

The pelagic ecosystem model used in this study was BIMS-ECO, which uses nitrogen as a currency and is based on the 1D model developed by Oguz et al. (2001). The model domain extended to 150 m depth and included 23 z-levels compressed towards the surface such that the vertical resolution increased from 2 m resolution near the surface to 20 m near the lower boundary. The model had 12 state variables (Fig. 2) consisting of two phytoplankton groups, small and large phytoplankton ( $P_f$ ,  $P_d$ ; smaller and larger than 10  $\mu\text{m}$ , loosely representing flagellates and diatoms), micro- and mesozooplankton ( $Z_s$ ; smaller than 0.2 mm and  $Z_l$  between 0.2 and 2 mm), bacterioplankton (B), labile pelagic detritus ( $D_p$ ), dissolved organic nitrogen ( $D_n$ ), nitrate (N), ammonium (A), the opportunistic heterotrophic dinoflagellate *Noctiluca scintillans* ( $Z_n$ ), and the gelatinous carnivores; *Aurelia aurita* ( $Z_a$ ), and *Mnemiopsis leidyi* ( $Z_m$ ). *Beroe ovate* ( $Z_b$ ) was parameterised as a grazing term on *M. leidyi*. *M. leidyi* was introduced into the model at the start of 1988. *M. leidyi* was first observed in the Black Sea during the early 1980s (Vinogradov et al., 1989; Studenikina et al., 1991; Shiganova, 1998) and was considered widespread by 1988 (Vinogradov et al., 1989) and *Beroe ovata* was introduced as a grazing term on *M. leidyi* at the beginning of 1998. *B. ovata*, was first recorded in the Black Sea in 1990 (Konsulov and Kamburska, 1998). By 1998 *B. ovata* was widespread throughout the Black Sea whence it became a key predator of *M. leidyi* (Vinogradov et al., 2000). Due to the dramatic impact invasive species had on the Black Sea during the PD time slice, the introduction of invasive species over the course of the simulation period was considered necessary in order to appropriately describe conditions at this time. The future (2080–2100) simulation was conducted using the post-1988 ecosystem model set-up. Nitrate flux from sediment suspension was parameterised on the north-western shelf at a constant

rate throughout all simulations. The model did not include oxygen as a state variable and did not explicitly resolve oxidation–reduction reactions at the anoxic interface. Because the model does not describe the oxidation of ammonia which is vital to the maintenance of the nitracline, a constant flux of nitrate was supplied to the model at 70 m depth. The pelagic ecosystem model was run offline using daily water temperature, salinity, horizontal and vertical velocities and vertical diffusivities output from the hydrodynamic model, and the same solar radiation fields used to force the hydrodynamic model. Nitrate initial conditions were set to the January climatological mean which was derived from CTD data obtained from the Black Sea database (produced following the NATO SFP ODBMS project; <http://sfp1.ims.metu.edu.tr>). A 5 year spin-up period allowed the biogeochemistry and ecosystem to adjust to the prevailing conditions.

#### 2.4. Assessment of atmospheric forcing and downscaling of the surface wind field

Substantial variability exists in the regional scale performance of the AOGCMs used in the IPCC AR4 and subsequent work (Wilby and Fowler, 2010). Hence, prior to conducting a dynamical downscaling study, the regional performance of the IPSL model from which surface forcing fields were extracted was assessed. We additionally assessed the regional performance of the ERA40 reanalysis in order to better understand the cause of any differences between the HC and PD simulations. The ERA40 heat flux data was found to be significantly correlated with observed SST records between 1980 and 2000, exhibiting realistic interannual and multiannual variability. The net surface heat input to the Black Sea between 1980 and 2000 was positive and almost identical in both the ERA40 and IPSL–CM4 (LU20C2) data sets.

Surface wind fields were assessed through comparison to satellite derived wind data using the Cross-Calibrated, Multi-Platform Ocean Surface Wind Velocity CCMP data product. Satellite derived wind speeds were 12% larger than those derived from the ERA40 reanalysis. Conversely, IPSL–CM4 (LU20C2) mean wind speeds were 340% larger than the CCMP wind fields, highlighting the limitations of the AOGCM. Consequently, a statistical downscaling approach was applied to adjust both the ERA40 and IPSL–CM4 mean wind speeds to contemporary observations. A bias removal downscaling approach was applied following

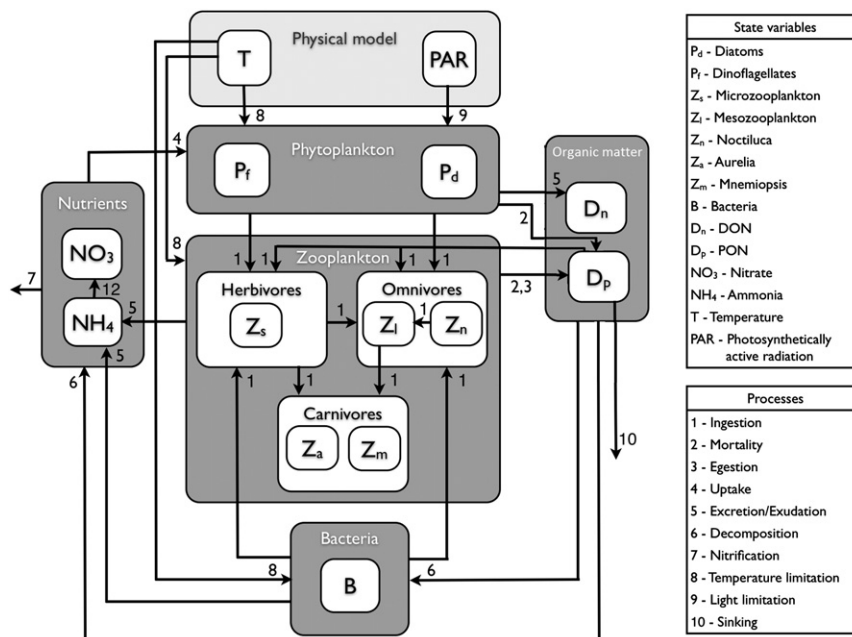


Fig. 2. Schematic diagram of BIMS\_Eco model setup and trophic interactions.

Eq. (1), where  $PD(t)$  represents the Present Day time series,  $FS(t)$  the A1B future scenario time series,  $ref$  the reference time series derived from observations,  $\langle \rangle$  indicates a multi-year temporal mean and  $*$  indicates the corrected (downscaled) time series.

$$PD^*(t) = PD(t) \langle ref \rangle / \langle PD \rangle \quad \text{and} \quad FS^*(t) = FS(t) \langle ref \rangle / \langle PD \rangle \quad (1)$$

The bias correction approach removes any spatial mean bias from the forcing fields but assumes that other statistical properties of the time series are acceptable. This approach also assumes that any bias remains constant over time.

### 2.5. Model validation approach

Due to a lack of data availability, a full statistical validation of the model variables was limited to Sea Surface Temperature (SST), surface chlorophyll concentration and water column properties which could be derived from CTD data (vertical structures of temperature, salinity, MLD and CIL properties). Simulated circulation fields were additionally compared qualitatively to published observations and simulated vertical profiles of nitrate were compared qualitatively to available cruise observations. Temperature, salinity, MLD and CIL properties (upper and lower boundaries and thickness) were compared to in situ measurements, utilising more than 1400 CTD stations from the Black Sea database. Mixed Layer Depth (MLD) was defined as the first depth below the surface at which the density change relative to the surface exceeded  $0.125 \text{ kg m}^{-3}$ . CIL upper and lower boundaries were defined by the  $8^\circ \text{C}$  isotherm. In order to estimate MLD and CIL properties, modelled density and temperature fields were first interpolated onto a 1 m resolution vertical grid. In addition to direct point-to-point comparisons, mean seasonal cycles of SST, MLD, and CIL characteristics, calculated by averaging all available data during each month, were also compared. A suite of metrics were generated from the model-data comparisons: mean errors (ME), root mean square errors (RMS), correlation coefficients (PC) and standard deviations (SD).

Modelled surface chlorophyll distributions were validated against SeaWiFS chlorophyll-a data (level-3, 8-day, 9 km) standard mapped data which is available from <http://oceandata.sci.gsfc.nasa.gov/SeaWiFS/L3BIN/>. Only two full years of SeaWiFS data were available for validation purposes within the time frame of this study (1998 and 1999). To further evaluate model performance in representing surface chlorophyll distributions over a range of spatial scales and variable concentrations, a wavelet-based spatial comparison technique was applied. This technique has an advantage over direct pixel-to-pixel comparisons in that the results are not influenced by model bias, as comparisons are made between quantiles defined according to the data range within each individual data set. This method was originally developed by Casati et al. (2004) and has since been applied to SST and surface chlorophyll hindcasts by Shutler et al. (2011) and Saux Picart et al. (2011). The methodology outlined below follows the enhancements proposed by Saux Picart et al. (2011) and the reader is referred to the original paper for more detail. Briefly, binary fields for the two respective data sets were defined over a range of threshold values by setting all data within a distribution map which exceeded the threshold to 1 and all other data to 0. In this study thresholds were defined by ranking the data and dividing it into six equal quantiles (such that each quantile represented the same percentage of the data). Binary difference maps were then produced by subtraction of the corresponding (model and data) binary maps within each quantile range. A 2-D Haar wavelet decomposition was performed on the binary difference maps and finally Mean Square Error (MSE) and model Skill Score (SS) were calculated for each level of decomposition, where SS was calculated as a function of MSE as follows;  $MSE \text{ as } SS = 1 - MSE / 2\epsilon(1 - \epsilon)$ , and  $\epsilon$  is the percentage of pixels in the binary difference map above the threshold of interest. Skill Score ranges from 0 to 1, with 1 indicating a perfect fit.

## 3. Results

### 3.1. Assessment of model performance

A comparison of the relative performance of the HC and PD simulations can be found in MEECE (2012), results are summarised here to provide the reader with an understanding of model skill. Statistics describing the relationship between HC and PD model solutions and in situ data are summarised using Taylor diagrams. Statistics generated by comparing observations to the nearest model grid point (Fig. 3a and b) reveal that the PD solution has less skill than the HC solution, particularly in the representation of CIL characteristics. This was in part because the PD simulation was forced by a free running atmospheric model (not constrained to real time in the representation of interannual variability) and in part due to a warm bias in the PD SST record which led to thinner than observed CIL thicknesses. Comparisons of mean seasonal cycles in SST, MLD, and CIL properties (Fig. 3c and d), however, revealed that both the HC and PD simulations represented the seasonality in the SST record, the formation and breakdown of the seasonal thermocline and the formation during winter and persistence during summer of the CIL.

Time series of basin mean differences (model minus observation) in surface chlorophyll concentration (1998–99) are presented in Fig. 4. Time series of mean errors in the HC and PD surface chlorophyll distributions during 1998 and 1999 ranged from  $-1.42$  to  $1.5 \text{ mg m}^{-3}$ , and averaged  $-0.01 \text{ mg m}^{-3}$  for the HC simulation, and ranged from  $-1.65$  to  $1.57 \text{ mg m}^{-3}$ , with an average of  $-0.13 \text{ mg m}^{-3}$  for the PD simulation. Hence the HC and PD solutions exhibited a similar level of skill in simulating phytoplankton biomass concentrations during the two year comparison period. Both model solutions exaggerated the amplitude of the seasonal cycle in surface chlorophyll concentration, with positive errors (model overestimation) during the spring and autumn bloom periods and negative errors (model underestimation) in between bloom periods. Wavelet decomposition of the surface chlorophyll record revealed that the model performed well at intermediate chlorophyll values with SSs for quantiles 2–5 exceeding 0.5 at all spatial scales and exceeding 0.8 in 90% of cases at spatial scales of more than 120 km. Model performance was reduced for the case of the lowest and highest quantile ranges, which exhibited large temporal fluctuations in model skill at all spatial scales. This revealed that much of the incurred error in the model representation of phytoplankton blooms resulted from a temporal rather than a spatial mismatch in bloom dynamics.

In comparing annual mean HC circulation fields to published observations, the following recognised characteristics of the Black Sea circulation were well represented by the model solutions; (i) the general cyclonic circulation with two sub-basin scale cyclonic gyres, (ii) anticyclonic circulation within the NW shelf, (iii) anticyclonic eddies inshore of the large-scale cyclonic circulation and (iv) bifurcation of the rim current near the southern tip of Crimea. Velocity magnitudes also compared well to observations; maximum rim current velocities within the upper 100 m approached  $1 \text{ m s}^{-1}$  (with maximum velocities of  $1.35 \text{ m s}^{-1}$  simulated at the shelf edge adjacent to the Sakarya river mouth) in good agreement with published ADCP data (BSC, 2008). The PD mean velocity structure by comparison exhibited a large anticyclonic gyre in the SE of the basin which extended as a narrow tongue towards the northern shore, creating a southerly flow along the eastern boundary of the basin. As this feature is not seen in observations or in the reanalysis forced control run we suggest that it is a consequence of the wind fields derived from the IPSL-CM4 model. A more sophisticated downscaling technique may be required to overcome this problem in future dynamical downscaling studies of the Black Sea.

The vertical nitrate distribution in the model compared well in qualitative comparisons to observed nitrate profiles (Fig. 5) although when considering the PD simulation the nitrate maxima extended over a broader depth range than observed. The seasonal depletion

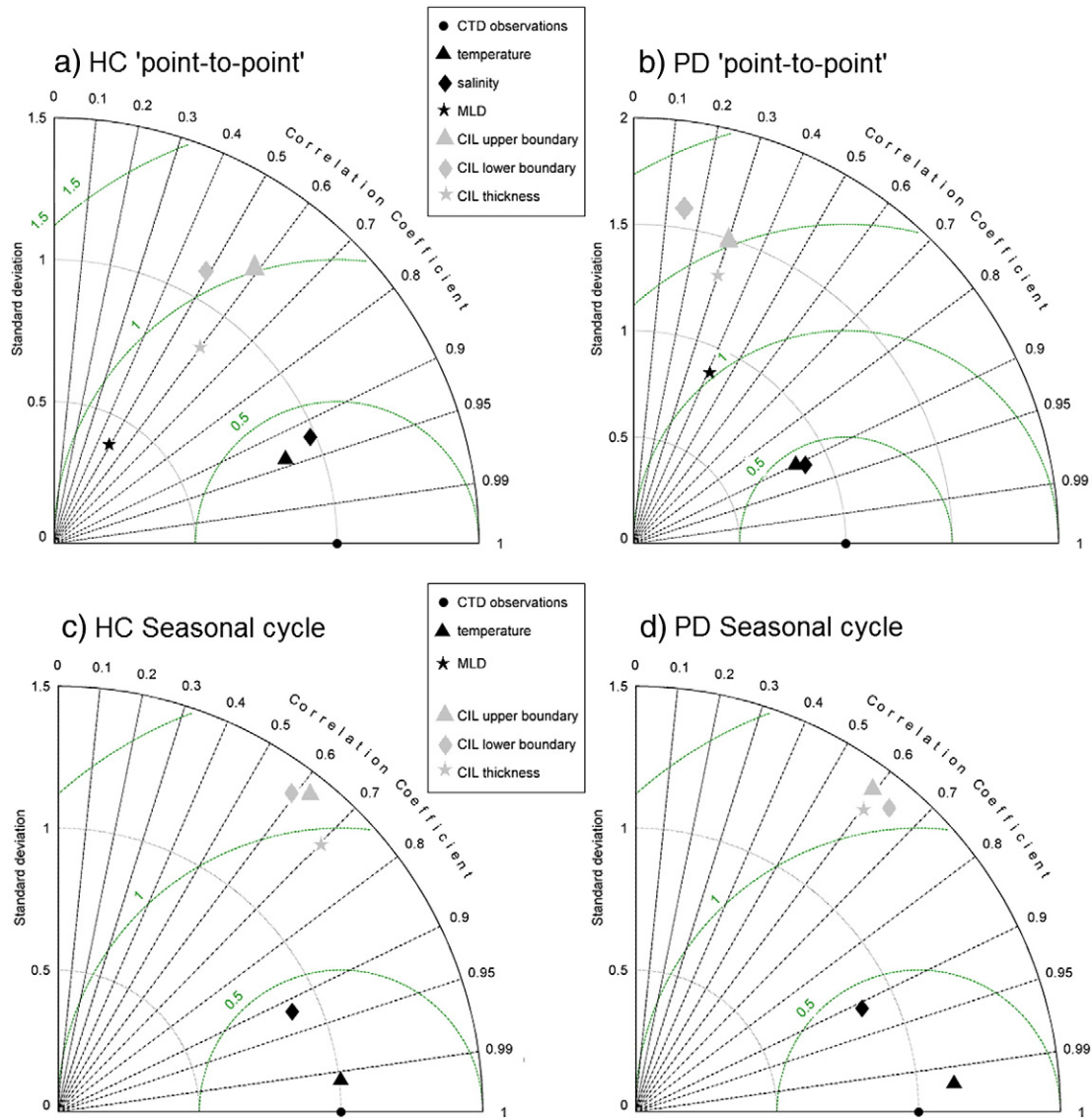


**Fig. 3.** Taylor diagrams illustrating the relative performances of the HC and PD solutions in simulation SST, SSS, MLD, and CIL upper and lower boundaries and thickness. In (a) HC and in (b) PD statistics generated from point-to-point comparisons, and in (c) HC and (d) PD statistics generated from comparisons of annual mean seasonal cycles.

and replenishment of nitrate within the upper water column was captured by the model.

### 3.2. Atmospheric drivers

In order to interpret projected changes in hydrographic conditions between the 20-year PD time slice (1980–2000) and the 20-year A1B time slice (2080–2100), we begin by summarising mean changes in atmospheric forcing variables. PD mean values and A1B minus PD differences in atmospheric variables are recorded in Table 2. Air temperature was projected to increase by 3.9 °C with an associated 8.5% increase in the surface sensible heat flux and the surface solar radiation was projected to increase by 9%. Evaporation was projected to increase by 14% and precipitation by 9%, causing a 172% increase in the net ocean to atmosphere freshwater flux. Wind stress over the Black Sea exhibited an 8% reduction on average and unlike other meteorological variables exhibited considerable spatial variability in response over the model domain. Wind speed increased in the north-west of the region and decreased in the south-east of the region. Changes in the spatial distribution of wind speed resulted in a 27% reduction in wind stress curl. As a consequence, upwelling velocities at the base of the mixed layer

( $w_E$ ) associated with divergent Ekman transport decreased by 13% on average. With regard to the tendency of the forcing to generate seasonal stratification, differences between spring and summer air temperatures and wind speeds are also of interest. The difference between spring (March/April) and summer (July/August) air temperature over the Black Sea decreased by 0.8 °C, while the fractional change in spring minus summer wind speed increased by 0.012 (Table 1).

### 3.3. Physical response

Mean values of key physical and biological variables simulated under PD and A1B climatic conditions are summarised in Table 2 along with the absolute or fractional change in the variable between the two time slices. Under PD conditions annual mean SSTs were lowest on the NW shelf and in the extreme east of the basin close to the Georgian coast, with the highest SSTs occurring in the deep regions of the eastern basin (Fig. 6a). The simulated mean change in SST (A1B minus PD) was 3.2 °C. There was little spatial variability in the annual mean warming trend which ranged from 3.1 °C to 3.4 °C (Fig. 6b). Maps of seasonal change in SST (Fig. 6c–f) show that SST increased during all seasons, with the largest increase during the summer months.

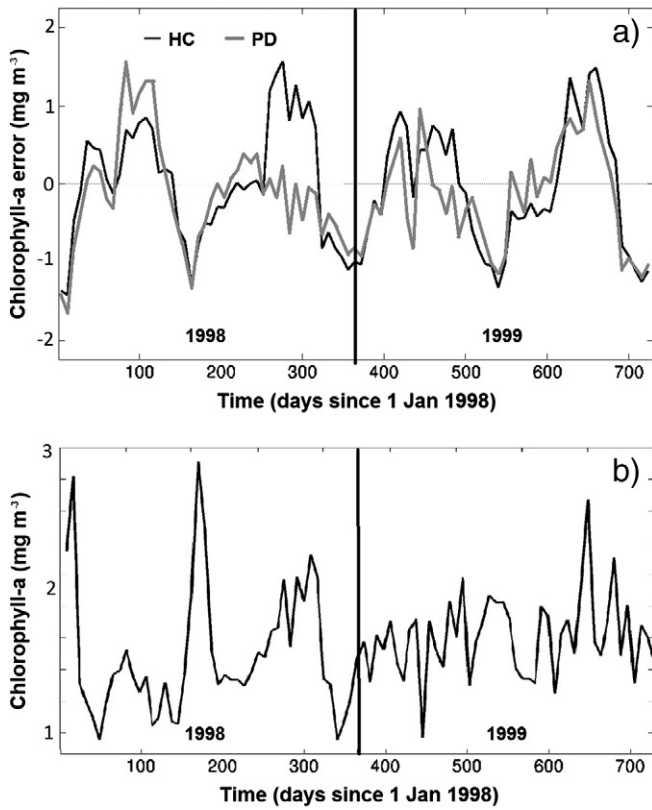


Fig. 4. (a) Mean differences in modelled surface chlorophyll distributions relative to SeaWiFS chlorophyll during 1998 and 1999. HC simulation errors are shown in black and PD simulation errors are shown in grey. (b) Basin averaged SeaWiFS chlorophyll concentrations during 1998 and 1999.

The impact of circulation on SST changes is evident during winter and spring, when shelf edge regions (associated with divergence and downwelling under PD conditions) warmed less than other regions. Winter SST, relevant to the formation of CIL water, showed the largest increases on the NW shelf and in the SE of the basin. Little change occurred in the timing or amplitude of the SST seasonal cycle (Fig. 6g).

Due to the strong shallow halocline in the Black Sea and strong riverine influences, sea surface salinities (SSSs) are low, ranging from less than 13 close to the Danube delta to a maximum value of 18.4 in the centre of the basin (Fig. 7a). Although salinity within the upper 20 m of the water column decreased on average, sea surface salinity exhibited a mean increase of 0.04 which was attributed to increased evaporation minus precipitation. There was much regional variability in the annual mean change in SSS (Fig. 7b), which ranged spatially from  $-2.8$  to  $4$ . The most pronounced increases in salinity occurred around the peripheral regions of the basin and in the east of the basin. There was a decrease in sea surface salinity within offshore regions of the western basin and in the region adjacent to the western shore of the Crimean Peninsula. Maps showing seasonal mean changes in SSS (Fig. 7c–f) reveal that freshening of the central western basin was most pronounced during the spring and summer months. The basin mean increase in SSS was most pronounced during the winter months (Fig. 7g).

PD (A1B) MLDs typically ranged from a summer mean of 7.1 m (6.7 m) to a winter mean of 56 m (53 m) respectively. Shallowing of the MLD suggests an increase in water column stability. A useful measure of water column stability is the Potential Energy Anomaly PEA ( $J m^{-3}$ ) which represents the amount of work required to bring about complete vertical mixing of the water column (e.g. Simpson and Bowers, 1981). In this work, the PEA of the upper 56 m of the water column (PEA-56) was considered as an indicator of the strength of the seasonal stratification. A depth of 56 m was chosen as this was the mean depth to which the water column became vertically mixed during winter. Under PD conditions, PEA-56 ranged seasonally from a minimum

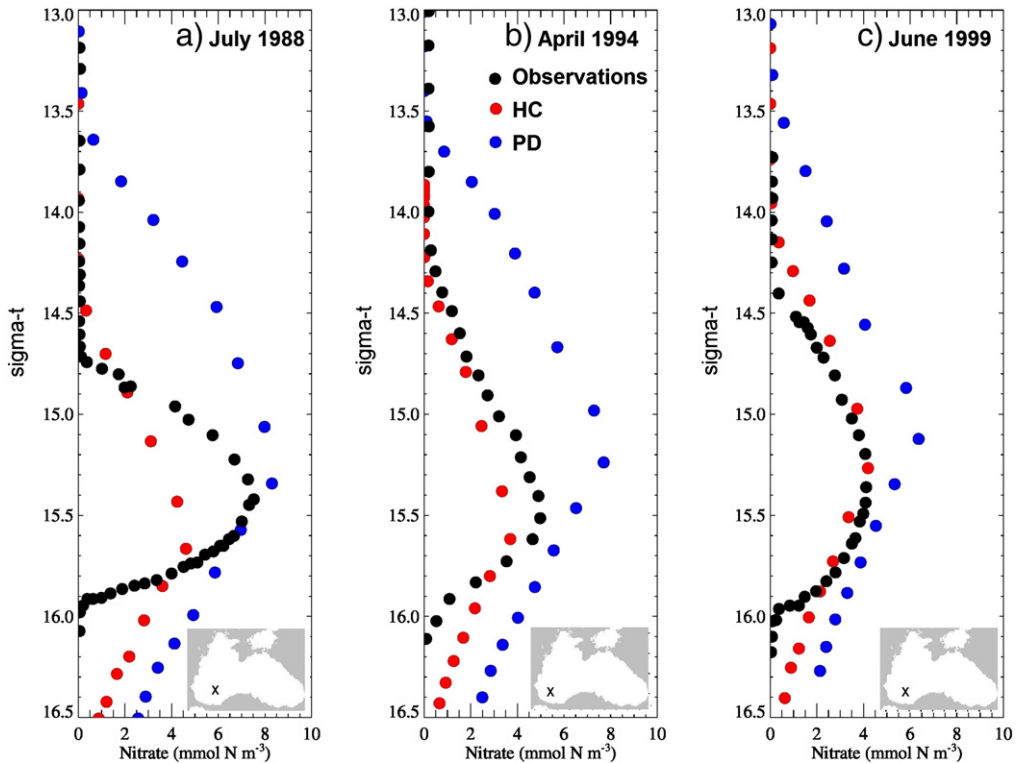


Fig. 5. A comparison of HC (red symbols), PD (blue symbols) and observed (black symbols) vertical nitrate profiles during (a) July 1988, (b) April 1994 and (c) June 1999. The locations of the profiles are indicated in the inset of each panel.

**Table 1**  
Mean differences (A1B [2080–2100] minus PD [1980–2000]) in meteorological forcing parameters extracted from the IPSL-CM4–V2 climate model (Marti et al., 2006) and averaged over the Black Sea.

Driver	PD (1980–2000)	A1B (2080–2100)	Change at A1B
Air temperature	11.5 °C	15.6 °C	+4.1 °C
Surface solar radiation	171.5 W m <sup>-2</sup>	183.3 W m <sup>-2</sup>	+11.8 W m <sup>-2</sup>
Wind stress (magnitude)	0.0204 N m <sup>-2</sup>	0.0189 N m <sup>-2</sup>	–8%
Wind direction	26.3°	26.5°	–
Wind stress curl	2.13 × 10E–8 Pa m <sup>-1</sup>	1.56 × 10E–8 Pa m <sup>-1</sup>	–27%
Evaporation	2.3E–8 m s <sup>-1</sup>	2.6E–8 m s <sup>-1</sup>	+14%
Precipitation	2.1E–8 m s <sup>-1</sup>	2.3E–8 m s <sup>-1</sup>	+9%
Evap. minus precip.	1.3E–9 m s <sup>-1</sup>	3.6E–9 m s <sup>-1</sup>	+172%

value of 27 J m<sup>-3</sup> in February to a maximum value of 164 J m<sup>-3</sup> in August, with the annual mean being 85 J m<sup>-3</sup>. Under A1B conditions PEA ranged seasonally from 34 J m<sup>-3</sup> to 216 J m<sup>-3</sup> with the annual mean being 107 J m<sup>-3</sup> (Fig. 8). The increase in PEA corresponded to an annual mean increase in the stability of the upper 56 m of the water column of 25%. The period of seasonal stratification, defined as the period of time over which PEA-56 exceeded 50 J m<sup>-3</sup>, increased in length from 167 days (46% of the year) during the PD simulation period, to 204 days (56% of the year) during the A1B simulation period.

The stability of seasonal thermal stratification is influenced by the difference between spring and summer air temperatures. Spring air temperature modulates the temperature of the water which becomes trapped below the seasonal thermocline. Summer air temperature influences the water temperature of the surface mixed layer during the stratified period. Hence, the difference between spring and summer air temperatures is related to the magnitude of the vertical temperature gradient across the seasonal thermocline (e.g. Holt et al., 2014). The reduction in summer minus spring air temperature in the atmospheric model is not, therefore, conducive to an increase in thermal stratification. Likewise, while decreased wind mixing during spring may hasten the onset of seasonal stratification, increased wind mixing during July and August is not conducive to enhanced stratification during these months. When comparing the SSS and PEA maps (Figs. 7 and 8) it is also evident that increased seasonal stratification cannot be attributed to freshening of the surface mixed layer, since regions of PEA increase overlap regions of SSS increase. There is, however, a positive feedback in the system which favours an increase in stratification, expressed through the nonlinear equation of state; at higher temperatures the same vertical temperature difference leads to a larger vertical density difference. As an example, PD August mean SSTs averaged 25.5 °C and a 12 °C temperature difference between the surface and 56 m depth was typical. This corresponds to a vertical density difference over the same depth range of 3.57 kg m<sup>-3</sup>. Taking the A1B August mean SST value of 29 °C and assuming the same vertical temperature difference gives a vertical density difference of 4.09 kg m<sup>-3</sup>. This equates to a 12.5% increase in the vertical density difference of the upper 56 m of the water column. This increase in the vertical density gradient inhibits vertical mixing and therefore enhances warming of the surface layer, further increasing vertical stratification.

**Table 2**  
Projected changes (A1B–PD) in basin mean values of SST, SSS, PEA, length of seasonal stratification, and fractional change ((A1B / PD) – 1) in nitrate concentration and depth integrated netPP, phytoplankton biomass, micro- and meso-phytoplankton biomass and zooplankton biomass.

Variable	PD (1980–2000)	A1B (2080–2100)	Change at A1B
SST	17.0 °C	20.2 °C	+3.2 °C
SSS	17.96	18.00	+0.04
PEA (upper 56 m)	85 J m <sup>-3</sup>	107 J m <sup>-3</sup>	+25%
Duration of seasonal stratification	167 days	204 days	+37 days
Depth integrated nitrate	554.3 mmol N m <sup>-2</sup>	543.0 mmol N m <sup>-2</sup>	–0.02
Phytoplankton biomass	2.64 gC m <sup>-2</sup>	2.78 gC m <sup>-2</sup>	0.052
Micro-/meso-phytoplankton	0.71/1.93 gC m <sup>-2</sup>	0.71/2.07 gC m <sup>-2</sup>	0.005/0.07
Zooplankton biomass	267.6 mgC m <sup>-2</sup>	264.1 mgC m <sup>-2</sup>	–0.01

The importance of warming relative to freshening as a cause of reduced mixed-layer density (and increased vertical stratification) is further demonstrated by calculating the proportion of the reduction in the density of the upper 30 m of the water column attributable to temperature and salinity independently. The annual mean density decrease due to warming alone (–0.232 kg m<sup>-3</sup>) was 8.4 time larger than the density decrease due to freshening alone (–0.036 kg m<sup>-3</sup>). Except a small number of grid cells adjacent to the Danube, Dniester and Dnieper rivers, temperature was the dominant driver of changes in upper layer density throughout all regions of the basin and during all seasons. Considering the above alongside the seasonal changes in temperature and salinity it is evident that the projected increase in stratification was primarily a consequence of ocean warming.

The distribution of CIL water is influenced by the mean circulation structure of the basin and the associated divergence or convergence of isopycnal surfaces as discussed previously. The CIL simulated under PD conditions is thickest in the vicinity of the shelf edge and thins towards the centre of the basin (Fig. 9a) in accordance with observations. The CIL was absent from a small region in the NE of the deep basin during the summer and autumn of each year. The CIL was thickest and also deepest during March (Fig. 9b) and gradually thinned and shoaled over the course of the summer, having a minimum volume and minimum depth in the water column during October. The period of CIL formation under PD conditions thus extended from November through March. Under A1B climatic conditions (Fig. 9c) the CIL was largely absent except in a narrow band near the western shelf edge. A small volume of CIL waters were formed during February and March and during the summer months the CIL became completely eroded (Fig. 9d). Hence our simulations project erosion of the CIL under an A1B emission scenario. This reduction in CIL formation was attributed primarily to increased winter temperatures (most pronounced on the NW shelf and close to the SE coast; both regions associated with the coolest winter SSTs during the PD simulation period). Freshening of the upper water column may also contribute to reduced CIL formation. However, changes in salinity are not considered to be a dominant driver of the reduction in CIL formation, since changes in salinity had only a small impact on surface density by comparison to changes in temperature.

The basin-scale circulation structure simulated under PD conditions was dominated by a basin-wide cyclonic gyre, with the strongest

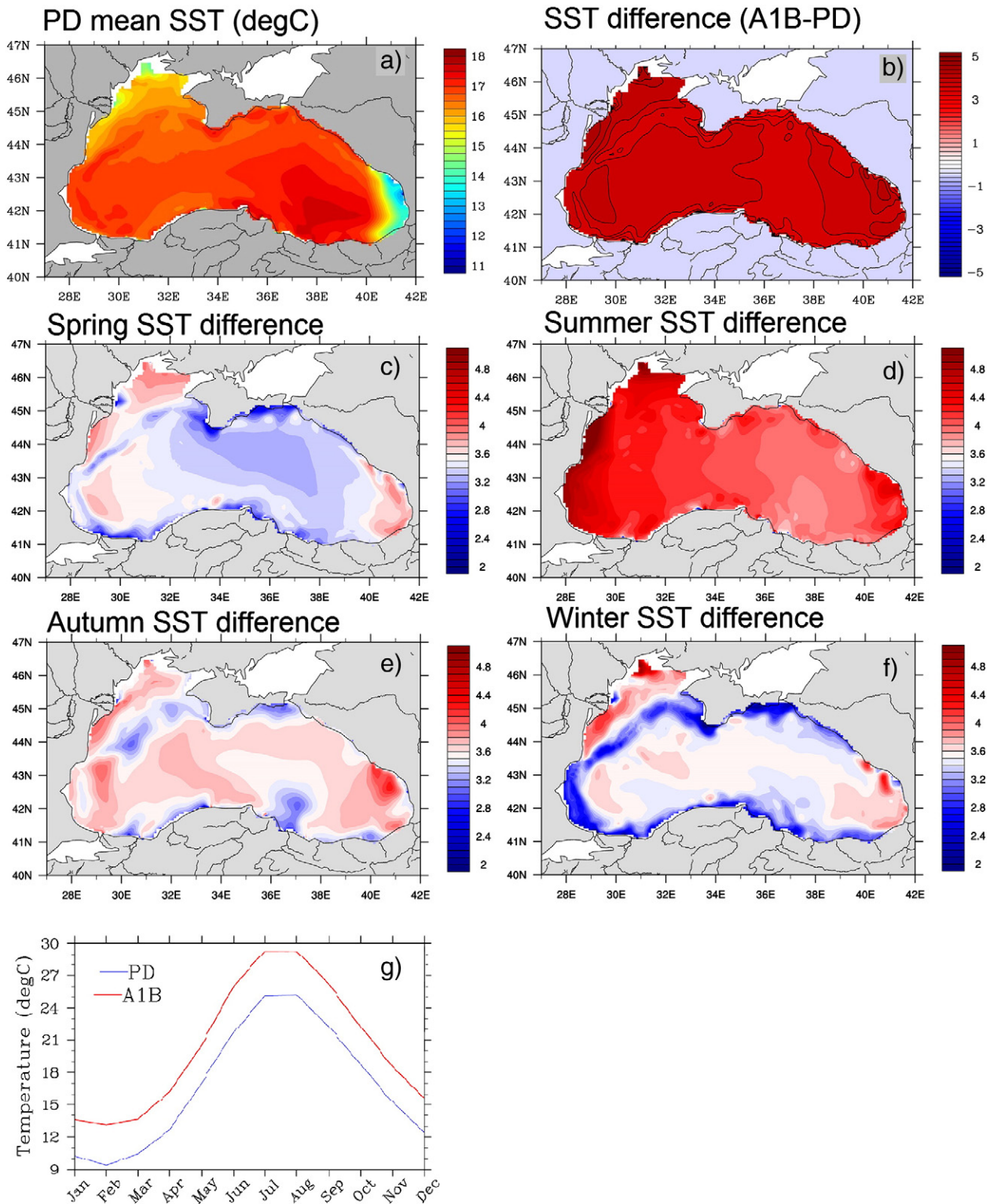


**Fig. 6.** (a) Mean PD distributions of SST, and changes (A1B–PD) in (b) annual, (c) spring (MAM), (d) summer (JJA), (e) autumn (SON), and (f) winter (DJF) mean SST, and in (g) a comparison of basin-mean PD (in blue) and A1B (in red) seasonal cycles of SST.

currents occurring at the shelf edge (Fig. 10a). In contrast, under A1B climatic conditions the mean basin-scale circulation exhibited anticyclonic circulation in the northern and eastern regions of the basin, with a weaker cyclonic circulation persisting in the southwest of the basin (Fig. 10b). The flow field simulated under A1B conditions was generally weak and meandering by comparison to the PD solution, with many

eddies. The anticyclonic circulation on the NW shelf persisted in the A1B simulation and another weak anticyclonic gyre was associated with the Bosphorus inflow. There was little difference between the PD and A1B surface wind stress fields when considered qualitatively (Fig. 10c and d). As noted previously, however, positive wind stress curl decreased significantly across large regions of the basin (Fig. 10e

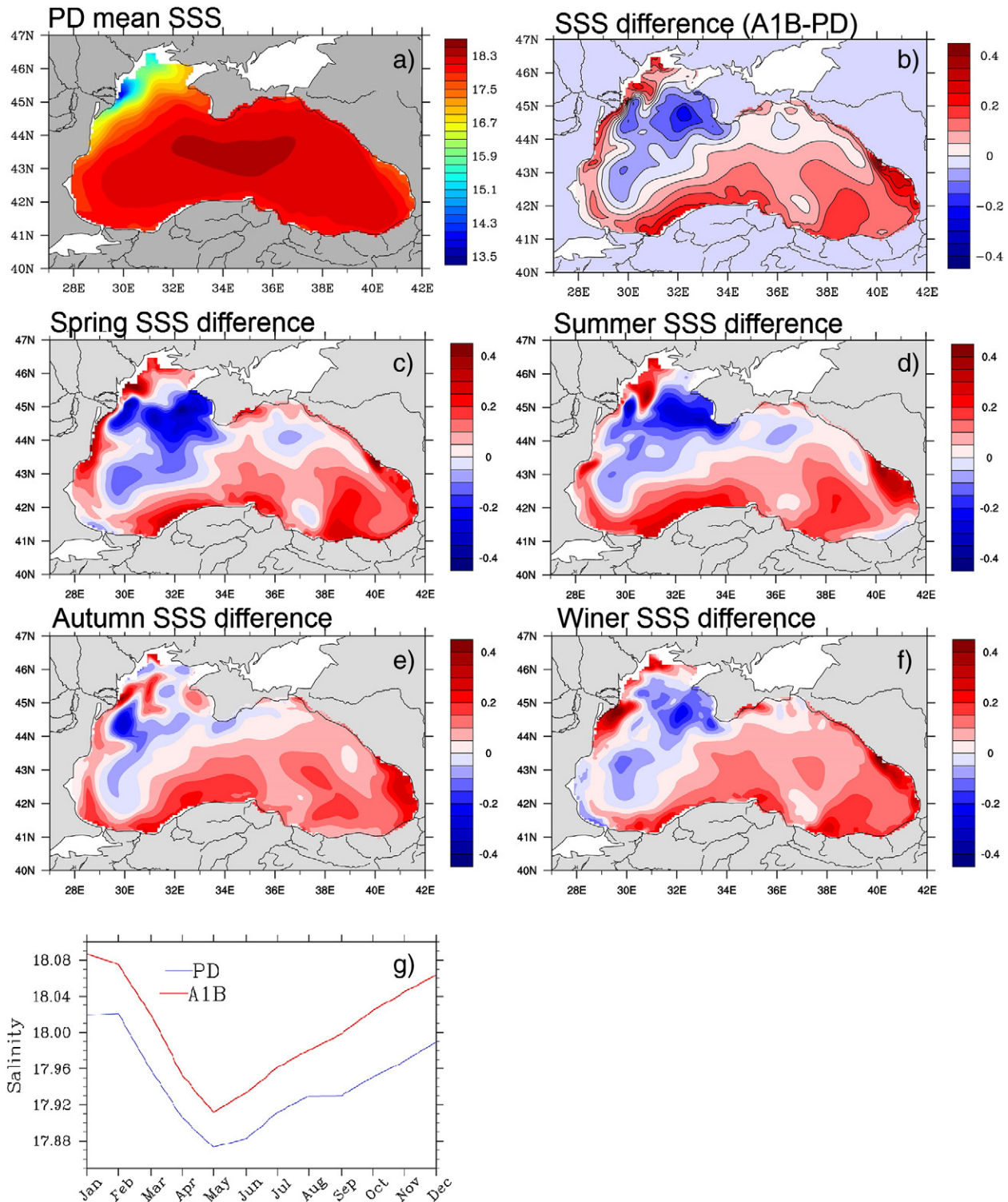


**Fig. 7.** (a) Mean PD distributions of SSS, and changes (A1B–PD) in (b) annual, (c) spring (MAM), (d) summer (JJA), (e) autumn (SON), and (f) winter (DJF) mean SSS, and in (g) a comparison of basin-mean PD (in blue) and A1B (in red) seasonal cycles of SSS.

and f). As wind stress curl is reported to be the dominant driver of the cyclonic circulation in the Black Sea (Korotaev et al., 2001; Ozsoy and Unluata, 1997; Stanev, 1990) the relaxation of the cyclonic circulation in the NW of the basin and the establishment of an anticyclonic dominated regime in the south and east of the basin was attributed to the 27% reduction in positive wind stress curl.

An E–W cross-section of salinity from the PD solution along 43.4 N (Fig. 11a) reveals upwelling in the centre of the cyclonic gyre (most

intense in the western side of the basin where the gyre is strongest) and downwelling in the peripheral regions of the basin. This type of circulation structure is conducive to the subduction of fresher waters near the shelf edge and the upwelling of more saline waters in the centre of the basin. Relaxation of the cyclonic circulation under the A1B scenario consequently resulted in an increase in surface salinity in peripheral regions and freshening near the centre of the gyre. The SSS maps (Fig. 7) also indicated a change in the advective distribution of fresh NW shelf

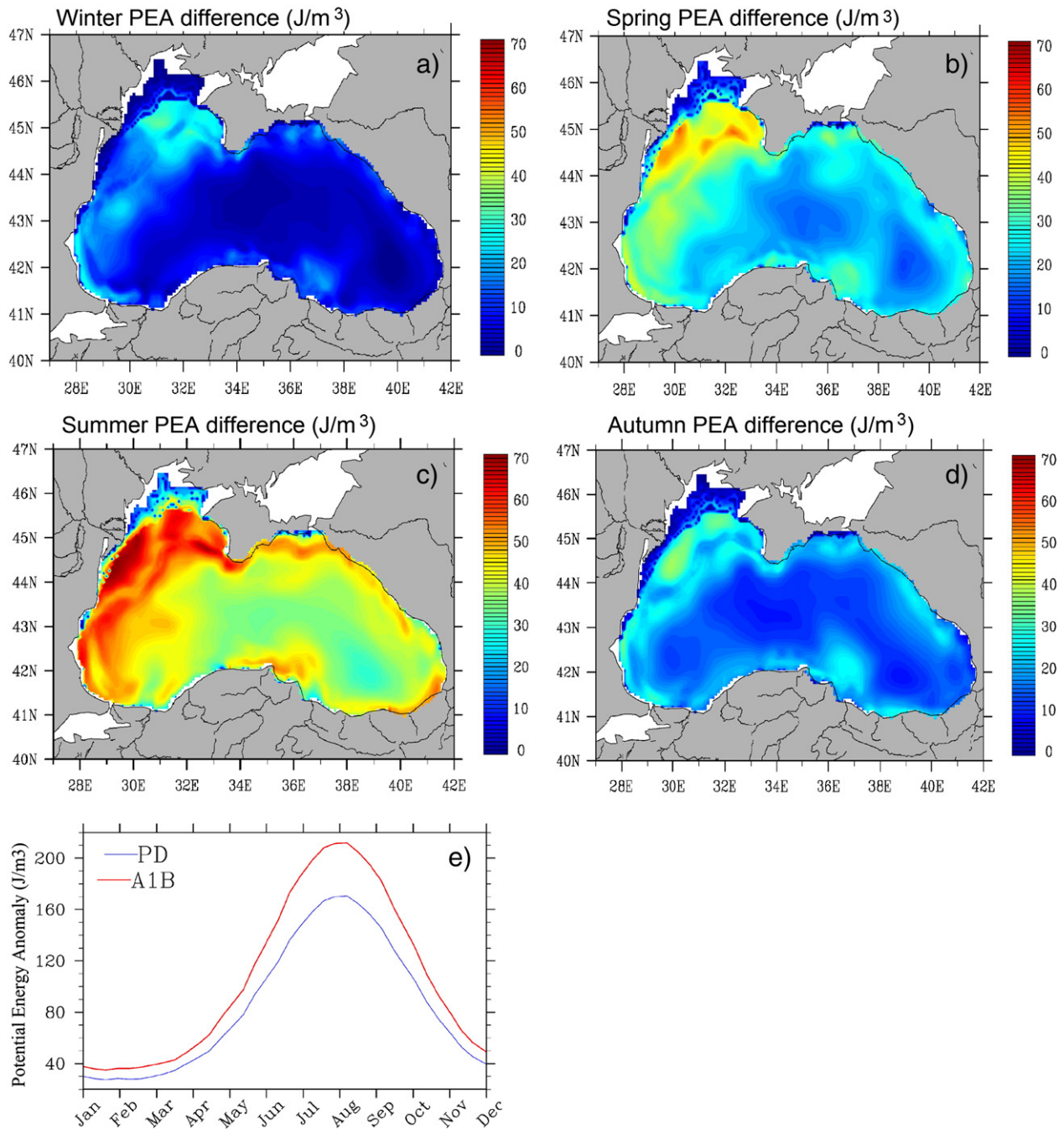


**Fig. 8.** (a) Maps showing the change in PEA of the upper 56 m of the water column (2080–2100 relative to 1980–2000) during (a) winter (DJF), (b) spring (MAM), (c) summer (JJA), and (d) autumn (SON) and in (e) 20-year mean seasonal cycles in PEA of the upper 56 m (PD simulation results in black and A1B simulation results in red).

waters under the A1B scenario. Under PD conditions the Danube plume was advected southwards by the rim current, which enhanced the southward extension of the buoyant plume (which under the influence of the earth's rotation formed a coastally trapped current). Conversely, under A1B climatic conditions the mean circulation resulted in an eastward advection of the plume towards the Crimean Peninsular. In this case the plume was no longer trapped by the coast and was able to spread further offshore.

The A1B salinity structure along 43.4 N is comparatively similar to the PD case (Fig. 10b), with a fresher surface layer, and increased upwelling in deep regions of the western basin. Analysis of the change (A1B–PD) in salinity along 43.4 N (Fig. 11c) revealed freshening of the upper 25 m of the water column between 30°E and 39.5°E, and an

increase in the salinity of the 25–50 m depth layer. The near-surface freshening trend resulted from an increase in the retention time of river waters within the surface layer and was most pronounced in regions influenced by the Danube plume. An increase in the retention time of river waters within the surface mixed layer may be attributed to three factors: (i) reduced subduction of riverine waters into the CIL, (ii) a reduction in vertical mixing due to the increased vertical stratification and reduced inputs of kinetic and potential energy, and (iii) reduced vertical Ekman transport. Freshening of the water column below 60 m depth in the east of the basin was a result of increased divergence and downwelling due to the shift from a cyclonic to an anticyclonic circulation structure in the region. Conversely, increased salinity within the western (cyclonic) region of the basin indicated increased

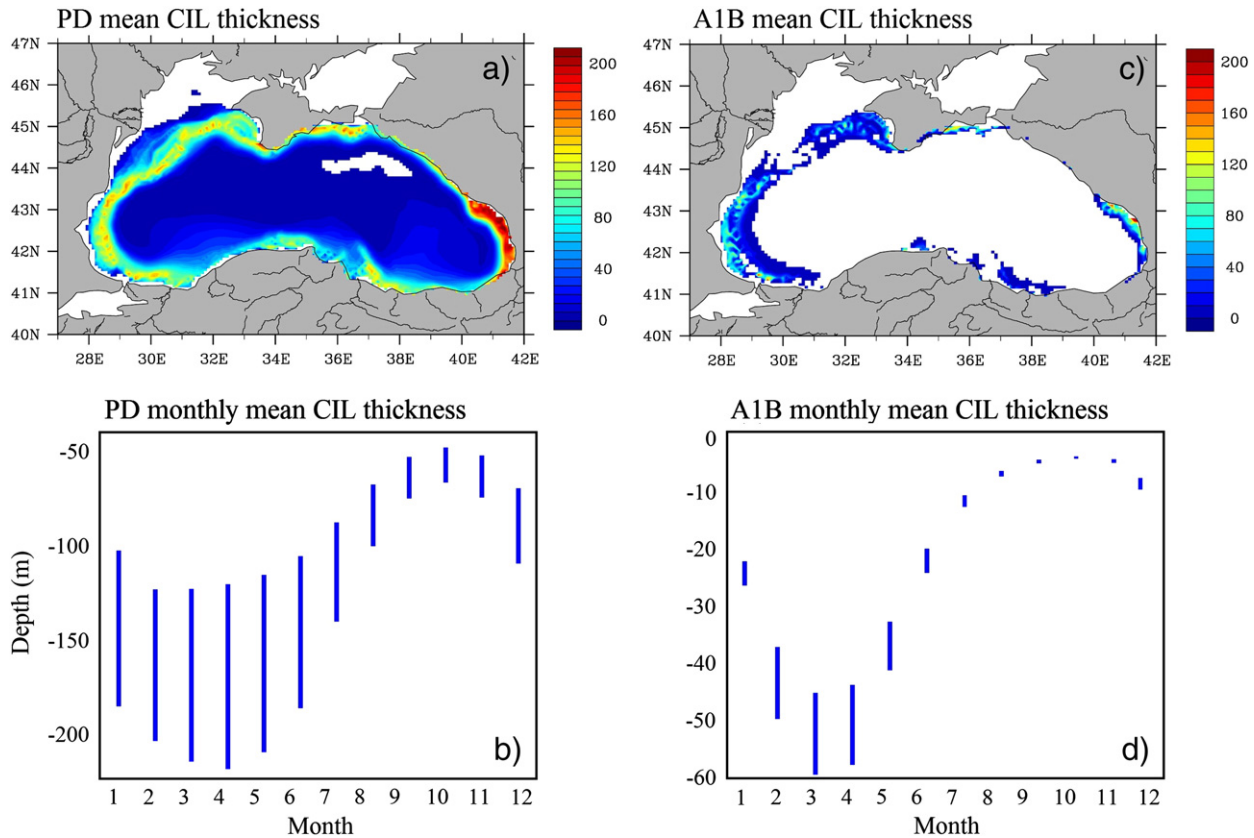


Fig. 9. Maps showing (a) PD and (b) A1B annual mean CIL thicknesses averaged over the entire basin. Blank areas indicate an absence of the CIL during part of the year.

upwelling in this region. The co-occurrence of anticyclonic circulation in the eastern basin and cyclonic circulation in the western basin resulted in an upward inclination of isobars towards the west coast of the basin. This, together with relaxation of the cyclonic circulation resulted in a significant increase in coastal upwelling along the Romanian and Bulgarian coast under A1B climatic conditions.

### 3.4. Physical controls on nitrate distribution

Throughout this paper projected changes in nitrate and lower trophic level (LTL) variable concentrations are expressed in terms of fractional change, defined as  $(A1B_{(2080-2100)} / PD_{(1980-2000)}) - 1$ , following Holt et al. (2012). Values of  $-1$  to  $0$  indicate a projected decrease in concentration under the future A1B scenario, while positive values indicate a projected increase in concentration.

Due to the heavy nitrate load of the Danube, Dnieper and Dniester rivers, simulated depth integrated nitrate concentrations on the NW shelf were extremely high, exceeding  $800 \text{ mmol N m}^{-2}$  close to the Danube delta (Fig. 12a). The basin mean fractional change in depth integrated nitrate concentration between the two time slices was  $-0.02$ . There was, however, a 4% increase in nitrate concentration within the upper 20 m of the water column (decreasing to 2% when averaged over the upper 35 m of the water column). Hence, while depth integrated nitrate concentration decreased, nitrate availability within the euphotic zone increased. A reduction in the vertical supply of nitrate from the nitracline to the euphotic zone was expected under A1B climatic conditions due to reduced vertical mixing and a reduction in Ekman pumping as noted previously. The increase in nitrate concentration within the upper 30 m of the water column was therefore attributed to the increased retention of riverine nutrients within the surface layer, an idea supported by the reduction in the salinity of this layer. The fractional change in nitrate concentration ranged spatially from a

minimum value of  $-0.93$  to a maximum value of  $1.1$  (Fig. 12b). There was an increase in depth integrated nitrate concentration throughout much of the northern Black Sea basin, which was most pronounced near the Crimean Peninsula. Nitrate concentration decreased in a small region within the south-east of the basin and in large parts of the western basin, with the largest decrease in the region adjacent to the Bulgarian coast.

Regional changes in depth integrated nitrate were dominated by changes which occurred in the upper 30–40 m of the water column due to changes in the advective distribution of river water. Below 40 m depth there was no obvious signal associated with the distribution of river discharges, rather changes to the horizontal distribution of nitrate resulted from changes in the large-scale circulation and the associated isopycnal redistribution of water. E–W cross-sections of PD (Fig. 11d) and A1B (Fig. 11e) nitrate concentrations along  $43.4 \text{ N}$  exhibited thickening of the nitracline in the centre of the cyclonic gyres and relatively high surface nitrate concentrations in the west of the basin, where the influence of river water was greatest. The change in nitrate concentration along  $43.4 \text{ N}$  at A1B as compared to PD (Fig. 11f) revealed a reduction in nitrate concentration west of  $32^\circ \text{ E}$ , and an increase in nitrate concentration in the east of the basin.

### 3.5. Lower trophic level response

Because of increased uncertainties associated with simulating higher trophic levels, an emphasis was placed on interpreting physical controls on primary production. Changes in phytoplankton biomass and zooplankton biomass are also summarised. Depth integrated primary production was greatest in the west of the basin, particularly on the NW shelf (Fig. 12c), where values reached  $950 \text{ mgC m}^{-2} \text{ day}^{-1}$  close to the Danube delta. This was primarily due to the influence of the nutrient rich rivers entering the NW shelf. Enhanced upwelling in the west of the

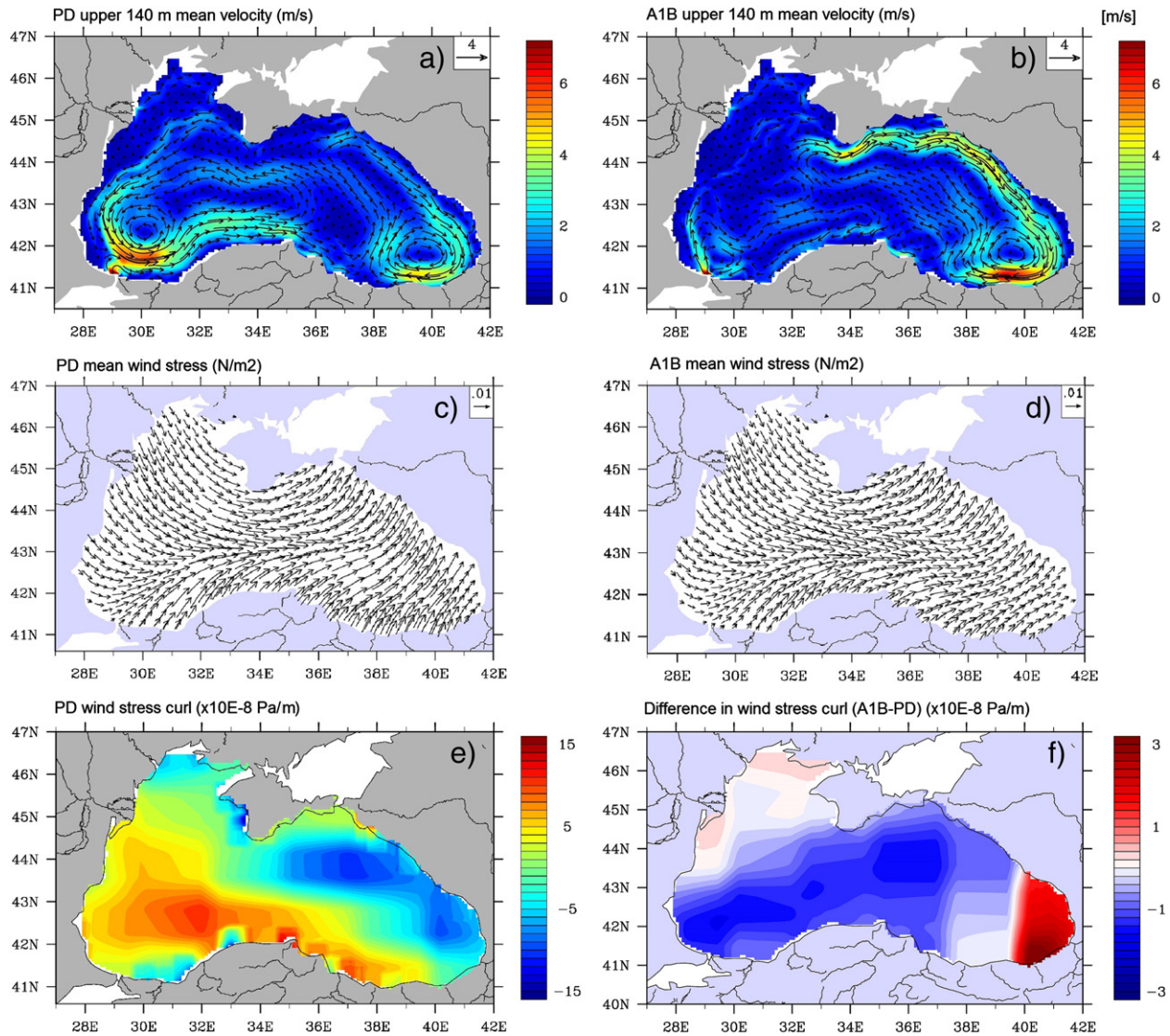


**Fig. 10.** (a) PD and (b) A1B annual mean velocity fields integrated over the upper 140 m of the water column, (c) PD and (d) A1B mean wind stress fields, (e) PD mean vertical component of positive wind stress curl and (f) difference (A1B–PD) in positive wind stress curl.

basin associated with the divergent cyclonic circulation also supported lower levels of production away from shelf areas. Local peaks in production can be seen near the mouths of the Turkish and Georgian rivers. The basin mean fractional change in netPP between the A1B and PD time slices was 0.052. This increase was attributed to two factors (i) an increase in nitrate availability within the euphotic zone due to the increased retention of nutrient rich riverine water within the surface mixed layer, and (ii) a reduction in light limitation due to a 9% increase in surface solar radiation. The response of netPP to the climate scenario forcing was highly regional, with fractional change values ranging from  $-0.81$  to  $1.9$  (Fig. 12d). NetPP increased throughout much of the northern and eastern Black Sea basin, with the most pronounced increase in the region surrounding the Crimean Peninsula. There was a decrease in netPP in the southwest of the basin. The regional pattern of change in netPP approximately corresponded to the projected regional change in nitrate concentration. Mean seasonal cycles of netPP (Fig. 13) show that under PD conditions, netPP was sustained at a relatively constant rate between the months of February and August, with only a small reduction during June. The rate of primary production peaked at  $250 \text{ mgC m}^{-2} \text{ month}^{-1}$  during July and began to decline during September, reaching about 35% of the seasonal maximum during December. The A1B simulation showed similar seasonal variability

with a more pronounced bloom during July and August (production peaked at  $290 \text{ mgC m}^{-2}$  in July).

The comparison of PD and A1B phytoplankton and zooplankton biomasses was complicated by the introduction of new (invasive) species to the model structure over the course of the PD simulation period. As a consequence annual mean time series of phytoplankton and zooplankton biomasses were not stationary over the PD timeslice. Annual mean values of depth integrated phytoplankton increased from  $3270 \text{ mgC m}^{-2}$  in 1980 to a maximum value of  $3800 \text{ mgC m}^{-2}$  in 1995, and subsequently levelled off with a value of  $\sim 3700 \text{ mgC m}^{-2}$  between 1995 and 1999. The increase in phytoplankton biomass was attributed to a decline in zooplankton biomass, which decreased from an annual mean of  $490 \text{ mgC m}^{-2}$  in 1987 to  $295 \text{ mgC m}^{-2}$  in 1988 (Fig. 12b). This reduction in zooplankton biomass was due to the spread and subsequent blooming of *M. leidy*, which graze on zooplankton. In order to compare PD and A1B time slices it was therefore necessary to shorten the PD time slice including only the period from (1988–2000).

The mean fractional change in total phytoplankton biomass (A1B relative to PD) was 0.054, this value ranged spatially from  $-0.53$  to  $1.1$ . The A1B time slice was characterised by higher phytoplankton biomass in the north of the basin and lower phytoplankton biomass in the southwest of the basin relative to the PD time slice (Fig. 12f). Projected

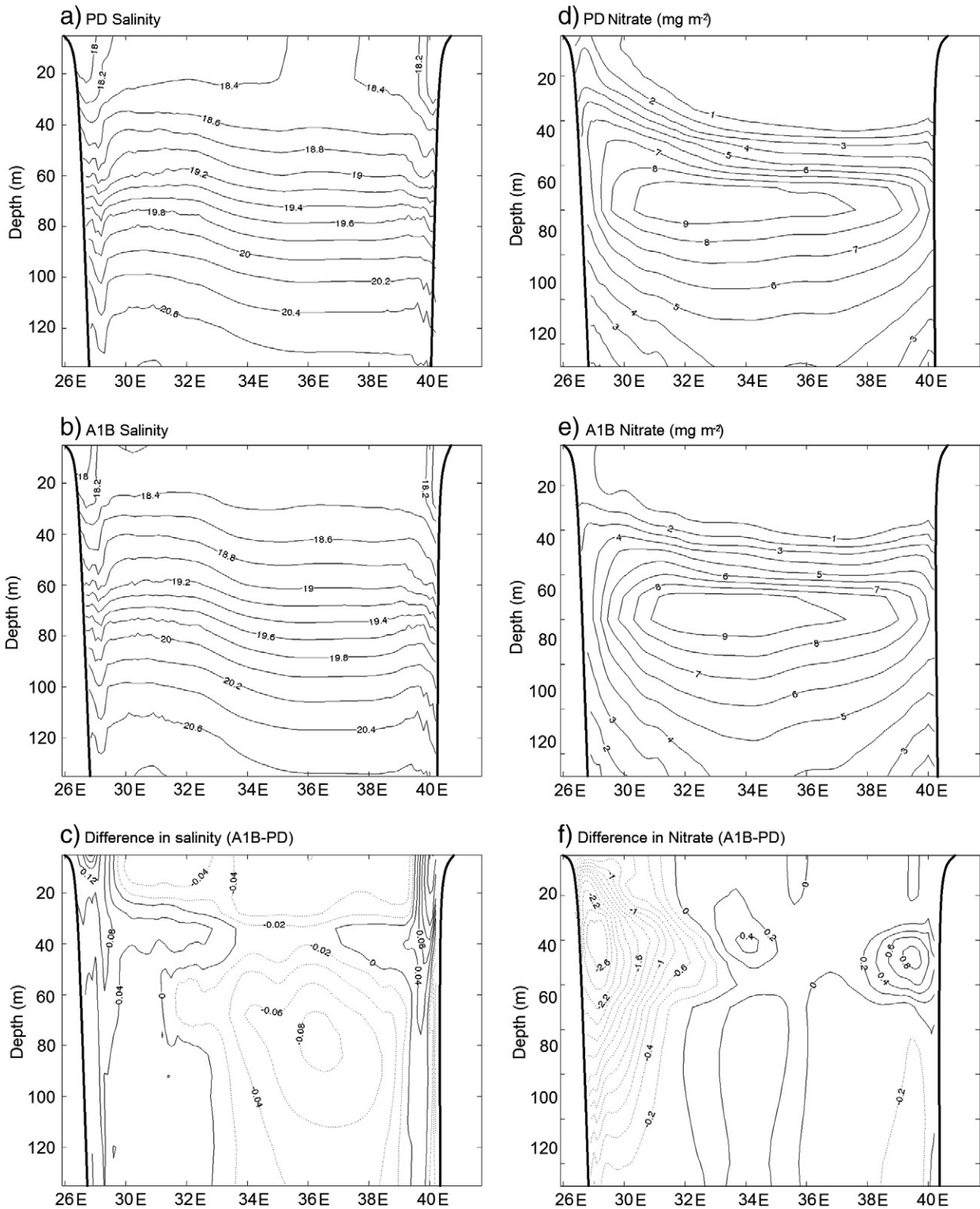


**Fig. 11.** (a) PD and (b) A1B E-W transects of salinity along 43.4 N, and (c) difference in salinity (A1B-PD), (d) PD and (e) A1B E-W transects of nitrate along 43.4 N and (f) difference in nitrate (A1B-PD).

changes in the distribution of phytoplankton biomass reflected the changes in the distribution of netPP and nitrate. Both the PD and A1B simulations exhibited two seasonal peaks in phytoplankton biomass, the first occurring during March and April, and the second during August, with a trough during June and low biomass values between October and January (Fig. 13b). Under A1B climatic conditions a more pronounced seasonal cycle was obtained, with higher biomass during

the bloom periods and lower biomass during January/February and June. The peak bloom biomass values changed between the simulations (decreasing from 680 mgC m<sup>-2</sup> to 500 mgC m<sup>-2</sup> during February, increasing from 530 mgC m<sup>-2</sup> to 740 mgC m<sup>-2</sup> during June and from 220 mgC m<sup>-2</sup> to 560 mgC m<sup>-2</sup> during September). As the seasonal cycle of phytoplankton biomass differed from the seasonal cycle of primary production, it was evident that the seasonality in phytoplankton

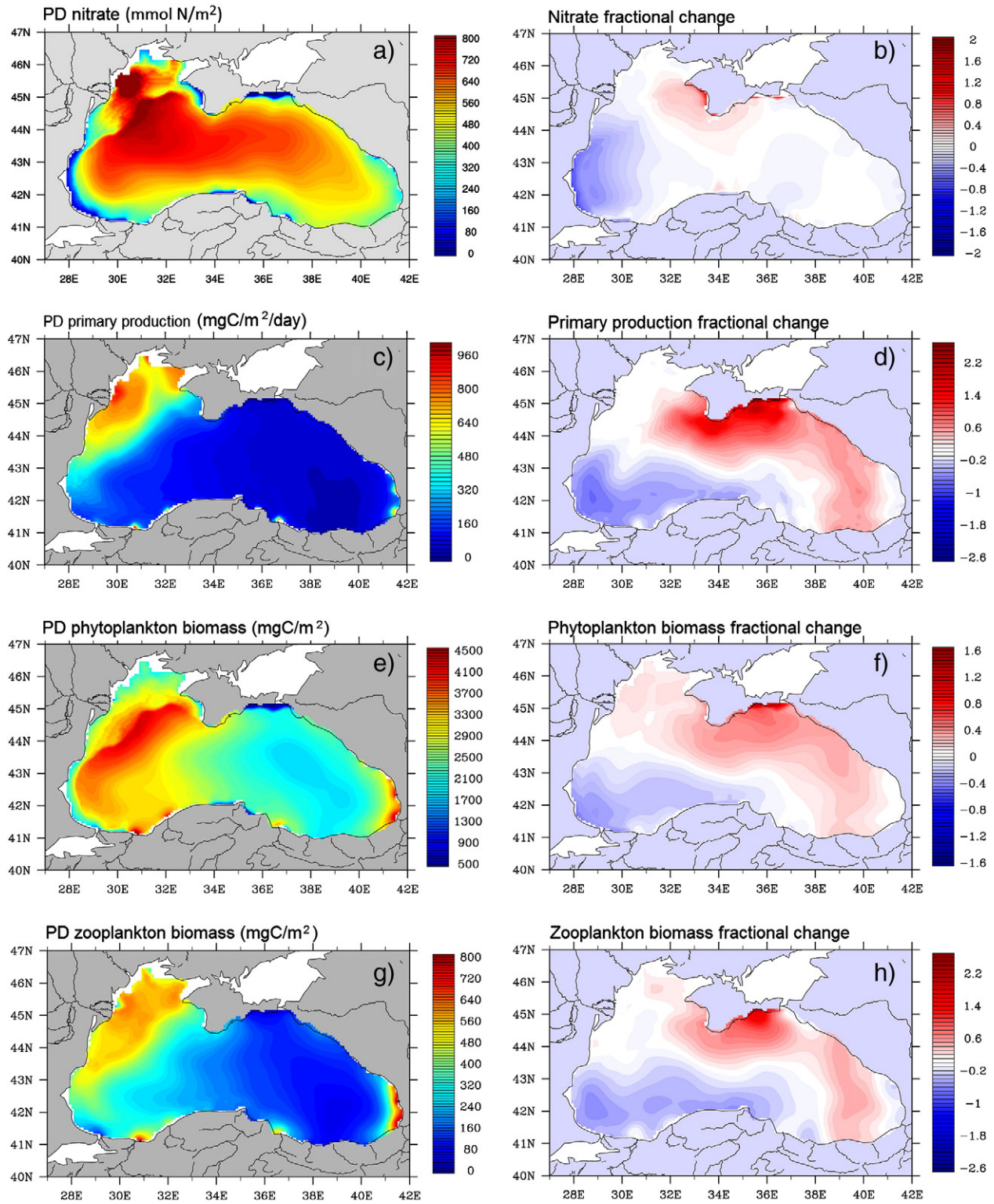


**Fig. 12.** PD mean concentration and fractional change  $[(A1B / PD) - 1]$  in depth integrated (a and b) nitrate concentration, (c and d) net primary production, (e and f) phytoplankton biomass, and (g and h) zooplankton biomass.

biomass was strongly influenced by the balance between growth and grazing pressures.

To elucidate the changes seen in total phytoplankton biomass, it is useful to consider the changes in small and large phytoplankton biomasses individually. Small phytoplankton biomass increased in the central and northern basin, particularly in the region adjacent to the Crimean Peninsula (Fig. 14a) having a mean fractional change of 0.005

and a spatial range in fractional change of  $-0.38$  to  $1.1$ . The mean fractional change in large phytoplankton biomass was  $0.07$ , and this value ranged spatially from  $-0.71$  to  $2.1$ . Large phytoplankton biomass increased throughout the north and east of Black Sea and decreased in the southwest (Fig. 14b). Hence, the overall trend of increasing phytoplankton biomass in the northern and eastern Black Sea and decreasing biomass in the south-eastern Black Sea was attributed predominantly to

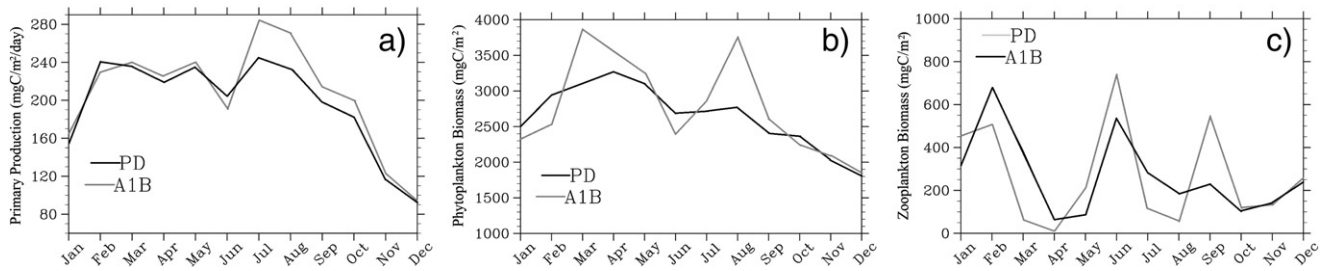


Fig. 13. Mean seasonal cycles (PD black lines and A1B grey lines) of depth integrated (a) net primary production, (b) phytoplankton biomass and (c) zooplankton biomass.

changes in large phytoplankton biomass, which respond positively to higher nutrient environments. The small phytoplankton group in the Black Sea is largely comprised of dinoflagellates, while the large phytoplankton group is largely composed of diatoms. Hence our results suggest an increase in diatom fraction on the NW shelf and in the eastern basin of the Black Sea under an A1B climate scenario.

No significant fractional change in basin averaged zooplankton biomass was projected. However, there was a significant change in the spatial distribution of zooplankton biomass (Fig. 12g and h), which approximately mirrored the spatial changes in phytoplankton biomass. The seasonality in zooplankton biomass reflected predator-prey interactions between phytoplankton, zooplankton and *M. leidyi*. High levels of primary production during February, May and August triggered zooplankton blooms which were typically short lived due to top down control.

#### 4. Discussion and conclusions

The projected physical response of the Black Sea to the imposed future climate scenario can be summarised as warming of the water column above the permanent pycnocline, an increase in the strength and duration of seasonal stratification, erosion of the CIL, relaxation of the cyclonic circulation in the northwest of the basin and reversal of the cyclonic circulation in the southeast of the basin. As surface warming is projected with a relatively high degree of confidence in the present generation of climate models (Randall et al., 2007), warming of the Black Sea upper layer, increased water column stability, and erosion of the CIL are believed to be robust results of this study. Changes in the hydrological cycle are highly uncertain in the present generation of climate models. A high degree of uncertainty is also associated with projecting changes in the atmospheric circulation, particularly at regional scales (e.g. Lowe et al., 2009). Consequently, the regional wind fields for a relatively small area such as the Black Sea may vary considerably between different AOGCMs, inferring that the results of dynamical downscaling studies may be strongly dependent on the choice of global model from which atmospheric forcing is

derived. Additionally, the results are dependent on the choice of statistical downscaling technique applied to the surface wind stress field. If a delta-change approach to downscaling had been adopted in this study rather than the bias correction approach, spatial variability in the wind forcing field would have remained unchanged between the two timeslices. As a consequence, the spatial patterns of change in nitrate concentration and lower trophic level variables projected in this study would have likely been very different. This study thus highlights the potential sensitivity of downscaled climate modelling studies to the choice of wind forcing fields and further demonstrate how a relatively small change in the mean wind stress field may dramatically change the basin-scale circulation of enclosed basins such as the Black Sea, with significant consequences for biophysical interactions.

CIL formation is believed to be the most important mechanism for the ventilation of the lower reaches of the oxic zone and as such erosion of the CIL has significant consequences for biogeochemical cycling in the Black Sea. If the rate of ventilation does not balance the rate of oxygen consumption, shoaling of the upper boundary of the suboxic zone can be expected. This process has already been observed over interannual and multiannual time scales. Kononov et al. (2005) demonstrated a linear relationship between CIL core temperature and oxygen concentration over interannual timescales, and reported that anomalously cold years are associated with elevated oxygen concentrations within the CIL. As this study employed a relatively simple ecosystem model which did not include oxygen as a state variable or explicitly resolve oxidation and reduction processes at the anoxic interface, the consequences of changes in ventilation associated with a reduction in CIL volume can only be indirectly inferred.

At the basin-scale, nitrate concentration within the euphotic zone of the Black Sea was projected to increase, fuelling an increase in primary production. This occurred despite a reduction in the vertical supply of nitrate from the nitracline to the euphotic zone due to reduced vertical mixing and reduced Ekman pumping. The increase in nitrate availability in the euphotic zone was thus attributed to an increase in the retention time of riverine waters within this layer. We propose that reduced CIL formation, alongside reduced vertical mixing and reduced Ekman

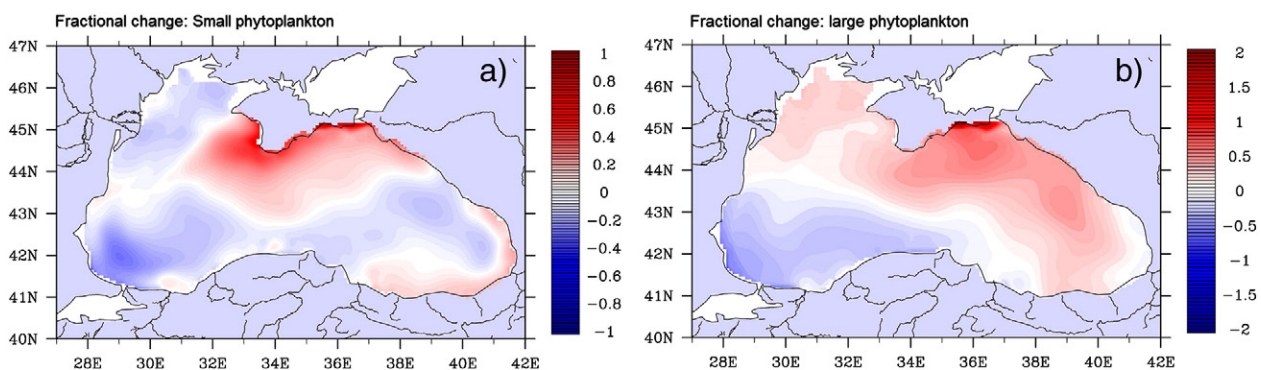


Fig. 14. Fractional change  $([A1B / PD] - 1)$  in (a) small phytoplankton biomass and (b) large phytoplankton biomass.

pumping, played a significant role in prolonging the residence time of nutrient rich river waters within the surface mixed layer under A1B climatic conditions. Determination of the relative contributions of each of these processes, however, requires further study. The importance of CIL formation in the subduction of river waters into the suboxic zone was first proposed by Tugrul and Salihoglu (2003). More recently, McQuatters-Gollop et al. (2008) suggested that the anomalously high phytoplankton biomass observed in the Black Sea during 2001 almost certainly resulted from climate induced processes and that the reduced subduction of nutrient rich surface waters into the CIL may have played an important role.

Eremeev et al. (1996) suggest that winter convective mixing provides a flux of nitrate to the euphotic zone, which is approximately equal to the annual load of nitrogen from the Danube river. Hence production in the Black Sea may be equally sensitive to changes in both advective processes and vertical mixing. For the case of the particular numerical experiment presented here, however, changes to the advective distribution of nutrient rich river water are shown to exert a stronger control on changes in primary production than results from changes in the vertical supply of nutrients from the nitracline. The increased retention of riverine nutrients within the euphotic zone under A1B climatic conditions suggests that climate warming may exacerbate the impact of eutrophication in the Black Sea.

Observations have revealed that anomalously warm years in the Black Sea are associated with anomalously high phytoplankton biomass, and differ from the norm in the occurrence of distinct spring and autumn blooms, examples being 2001 and 2010. The mechanisms of the observed change in phytoplankton seasonality during warmer years have not been described in the literature. It is likely, however, that changes in predator prey relationships due to top-down control, in addition to increased primary production, are responsible for this change (Oguz and Gilbert, 2006; Oguz et al., 2008). The growth rate of each life stage of *M. leidy* is highly dependent on temperature, and as a result warmer years are associated with a higher biomass of gelatinous species, resulting in increased grazing pressure on zooplankton and reduced grazing pressure on phytoplankton. Interestingly, the results of this experiment are in agreement with historical observations in that there is a tendency towards more pronounced spring and autumn blooms under the warmer A1B climate scenario. Understanding of the mechanism behind this change, however, requires additional work.

The numerical experiment described in this study considers only one potential future emission scenario, and a single AOGCM. This approach is useful to assess model sensitivity to climatic forcing, and to improve understanding of climatic controls on biophysical interactions but not for providing future climate projections. The results presented here may thus be considered as one of many possible future scenarios for the Black Sea. An ultimate goal in the development of this work is the definition of an envelope of potential responses to future climatic change, considering different emission scenarios and comparing a range of AOGCMs. Due to nonlinearities and feedbacks within the system, an assessment of ecosystem sensitivity to changes in climatic forcing cannot be achieved using a statistical study (e.g. Holt et al., 2014). Hence, despite their limitations, dynamical downscaling studies provide one of the few means through which we may assess the potential sensitivity of regional marine ecosystems to climate change.

## Acknowledgements

This work was funded by Theme 6 of the EC seventh framework programme through the Marine Ecosystem Evolution in a Changing Environment (MEECE no. 212085) Collaborative Project.

CCMP wind fields were obtained through the online PO.DAAC Ocean ESIP Tool (POET) at the Physical Oceanography Distributed Active Archive Centre (PO.DAAC), NASA Jet Propulsion Laboratory, Pasadena, CA, USA.

ECMWF ERA-40 data used in this project have been obtained from the ECMWF data server.

Black Sea river flux data was collated within the framework of the SESAME project, EC contract no. GOCE-036949, funded by the European Commission's Sixth Framework Programme under the priority 'Sustainable Development, Global Change and Ecosystems'.

The AVHRR Oceans Pathfinder SST data were obtained through the online PO.DAAC Ocean ESIP Tool (POET) at the Physical Oceanography Distributed Active Archive Centre (PO.DAAC), NASA Jet Propulsion Laboratory, Pasadena, CA, USA.

## References

- Allen, J.L., Aiken, J., Anderson, T.R., Buitenhuis, E., Cornell, S., Geider, R., Haines, K., Hirata, T., Holt, J., Le Quééré, C., Hardman-Mountford, N., Ross, O.N., Sinha, B., While, J., 2010. Marine ecosystem models for earth systems applications: the MarQUEST experience. *J. Mar. Syst.* 81, 19–33.
- Antonov, J.I., Seidov, D., Boyer, T.P., Locarnini, R.A., Mishonov, A.V., Garcia, H.E., Baranova, O.K., Zweng, M.M., Johnson, D.R., 2010. World Ocean Atlas 2009, volume 2: salinity. In: Levitus, S. (Ed.), NOAA Atlas NESDIS. 69.
- Blumberg, A.F., Mellor, G.L., 1987. A description of a three dimensional coastal ocean model. In: Heaps, N. (Ed.), Three Dimensional Coastal Ocean Models. A.G.U., Washington, pp. 1–16.
- BSC, 2008. State of the environment of the Black Sea (2001–2006/7). In: Oguz, T. (Ed.), Publications of the Commission on the Protection of the Black Sea against Pollution (BSC) 2008-3, Istanbul, Turkey.
- Casati, B., Ross, G., Stephenson, D.B., 2004. A new intensity scale approach for the verification of spatial precipitation forecasts. *Meteorol. Appl.* 11, 141–154.
- Doney, S.C., Ruckelshaus, M., Duffy, J.E., Barry, J.P., Chan, F., English, C.A., Galindo, H.M., Grebmeier, J.M., Hollowed, A.B., Knowlton, N., Polovina, J., Rabalais, N.N., Sydeman, W.J., Talley, L.D., 2012. Climate Change Impacts on Marine Ecosystems. 4, 11–37.
- Eremeev, V.N., Sovorov, A.M., Godin, E.A., Khaliolin, A.K., 1996. Statistical analysis of the location of the upper layer boundary of the hydrogen sulphide zone from multiannual data. In: Griffiths, R.C. (Ed.), Hydrochemistry and dynamics of the hydrogen sulphide zone in the Black Sea Part IV, UNESCO Reports in Marine Science. UNESCO, pp. 59–107.
- Halpern, B.S., Walbridge, S., Selkoe, K.A., Kappel, C.V., Micheli, F., D'Agrosa, C., Bruno, J.F., Casey, K.S., Ebert, C., Fox, H.E., Fujita, R., Heinmann, D., Lenihan, H.S., Madin, M.P., Perry, M.T., Selig, E.R., Spalding, M., Steneck, R., Watson, R., 2008. A global map of human impact on marine ecosystems. *Science* 319, 948–952.
- Halpern, B.S., Longo, C., Hardy, D., McLeod, K.L., Samhouri, J.F., Katona, S.K., Kleisner, K., Lester, S.E., O'Leary, J., Ranellietti, M., Rosenberg, A.A., Scarborough, C., Selig, E.R., Best, B.D., Brumbaugh, D.R., Chapin, F.S., Crowder, L.B., Daly, K.L., Doney, S.C., Elfers, C., Fogarty, M.J., Gaines, S.D., Jacobsen, K.I., Karrer, L.B., Leslie, H.M., Neeley, E., Pauly, D., Polasky, S., Ris, B., St Martin, K., Stone, G.S., Sumaila, U.R., Zeller, D., 2012. An index to assess the health and benefits of the global ocean. *Nature* 488, 615–620.
- Holt, J., Butenschon, M., Wakelin, S.L., Artioli, Y., Allen, J.I., 2011. Oceanic controls on the primary production of the northwest European continental shelf under recent past and potential future conditions. *Biogeosci. Discuss.* 8, 8383–8422.
- Holt, J., Butenschon, M., Wakelin, S.L., Artioli, Y., Allen, J.I., 2012. Oceanic controls on the primary production of the northwest European continental shelf: model experiments under recent past conditions and a potential future scenario. *Biogeosciences* 9, 97–117.
- Holt, J., Schrum, C., Cannaby, H., Daewel, U., Allen, I., Artioli, Y., Bopp, L., Butenschon, M., Fach, B.A., Harle, J., Pushpadas, D., Salihoglu, B., Wakelin, S., 2014. Physical processes mediating climate change impacts on regional sea ecosystems. *Biogeosci. Discuss.* 11, 1909–1975. <http://dx.doi.org/10.5194/bgd-11-1909-2014>.
- IPCC AR4, 2007. Climate change 2007. The physical science basis. Summary for policymakers. In: Alley, R., Berntsen, T., Bindoff, N.L., et al. (Eds.), Contribution of Working Group I to the Fourth Assessment Report of the Intergovernmental Panel on Climate Change.
- Ivanov, L.L., Besiktepe, S., Ozsoy, E., 1997. The Black Sea cold intermediate layer. In: Ozsoy, E., Mikaelyan, A. (Eds.), Sensitivity to change: Black Sea, Baltic Sea and North Sea NATO/ASI Ser. Kluwer Acad. Publ., Dordrecht, pp. 253–264.
- Kononov, S.K., Murry, J.W., Luther, G.W., 2005. Basic processes of Black Sea biogeochemistry. *Oceanography* 18 (2), 24–35.
- Konsulov, A.S., Kamburska, L.T., 1998. Ecological determination of the new *Ctenophora Beroe ovata* invasion in the Black Sea. *Proceedings of the Institute of Oceanology. Varna*, 2, pp. 195–198.
- Kopelevich, O.V., Sheberstov, S.V., Yunev, O., Basturk, O., Finenko, Z.Z., Nikonov, S., Vedernikov, V.I., 2002. Surface chlorophyll in the Black Sea over 1978–1986 derived from satellite and *in situ* data. *J. Mar. Syst.* 36, 145–160.
- Korotaev, G.K., Oguz, T., Dorofeyev, V.L., Demyshev, S.G., Kubryakov, A.I., Ratner, Y.B., 2001. Development of Black Sea nowcasting and forecasting system. *Ocean Sci.* 7, 629–649.
- Lancelota, C., Stanevab, J., Van Eeckhoutc, D., Beckers, J.M., Stanev, E., 2002. Modelling the Danube-influenced North-western continental shelf of the Black Sea. II: ecosystem response to changes in nutrient delivery by the Danube River after its damming in 1972. *Estuar. Coast. Shelf Sci.* 54, 473–499.
- Locarnini, R.A., Mishonov, A.V., Antonov, J.I., Boyer, T.P., Garcia, H.E., Baranova, O.K., Zweng, M.M., Johnson, D.R., 2010. World Ocean Atlas 2009, volume 1: temperature. In: Levitus, S. (Ed.), NOAA Atlas NESDIS. 71 (184 pp.).

- Longhurst, A., 1995. Seasonal cycles of pelagic production and consumption. *Prog. Oceanogr.* 36, 77–167.
- Lowe, J.A., Howard, T.P., Pardaens, A., Tinker, J., Holt, J., Wakelin, S., Milne, G., Leake, J., Wolf, J., Horsburgh, K., Reeder, T., Jenkins, G., Ridley, J., Dye, S., Bradley, S., 2009. UK Climate Projections Science Report: Marine and Coastal Projections. Met Office Hadley Centre, Exeter, UK.
- Ludwig, W., Dumont, E., Meybeck, M., Heussner, S., 2009. River discharges of water and nutrients to the Mediterranean and Black Sea: major drivers for ecosystem changes during past and future decades? *Prog. Oceanogr.* 80 (40271), 199–217.
- Ludwig, W., Bouwmann, A.F., Dumont, E., Lespinas, F., 2010. Water and nutrients fluxes from major Mediterranean and Black Sea rivers: past and future trends and their implications for basin scale budgets. *Glob. Biogeochem. Cycles* 24, GB0A13. <http://dx.doi.org/10.1029/2009GB003594>.
- Marti, O., Braconnot, P., Bellier, J.R.B., Bony, S., Brockmann, P., Cadule, P., Caubel, A., Denvil, S., Dufresne, J.L., Fairhead, L., Filiberti, M.A., Foujols, M.A., Fichet, T., Friedlingstein, P., Gosse, H., Grandpeix, J.Y., Hourdin, F., Krinner, G., Levy, C., Madec, G., Musat, I., Noblet, N.D., Polcher, J., Talandier, C., 2006. The new IPSL climate system model: IPSL-CM4. *Note Pole Model*. 26.
- McQuatters-Gollop, A., Mee, L.D., Raitsoy, D.E., Shapiro, G.L., 2008. Non-linearities, regime shifts and recovery: the recent influence of climate on Black Sea chlorophyll. *J. Mar. Syst.* 74, 649–658.
- Mee, L.D., 1992. The Black Sea in crisis — a need for concerted international action. *Ambio* 21 (4), 278–286.
- MEECE, 2012. D3.4 Synthesis Report for Climate Simulations. Part 3: Black Sea. EC FP7 MEECE. 212085. <http://www.meece.eu/Downloads/D3.1.pdf>.
- Meehl, G.A., Stocker, T.F., Collins, W.D., Friedlingstein, P., Gaye, A.T., Gregory, J.M., Kitoh, A., Knutti, R., et al., 2007. Global climate projections. In: Solomon, S., Qin, M., Manning, M., Chen, Z., Marquis, M., Averyt, K.B., Tignor, M., Miller, H.L. (Eds.), *Climate Change 2007: The Physical Science Basis. Contribution of Working Group I to the Fourth Assessment Report of the Intergovernmental Panel on Climate Change*. Cambridge University Press, Cambridge, United Kingdom and New York, NY, USA.
- Mikaelyan, A.S., Zatsepin, A.G., Chasovnikov, V.K., 2013. Long-term changes in nutrient supply of phytoplankton growth in the Black Sea. *J. Mar. Syst.* 117–118, 53–64.
- Murray, J.W., Kononov, S.K., Callahan, A., 2003. Nitrogen reductions in the suboxic zone of the Black Sea: new data and models. In: Yilmaz, A. (Ed.), *Oceanography of the Eastern Mediterranean and Black Sea: Similarities and Differences of Two Interconnected Basins*. TUBITAK Publishers, Ankara, Turkey, pp. 591–602.
- Nezlin, N.P., 2008. Seasonal and interannual variability of remotely sensed chlorophyll. *Environ. Chem.* 5Q, 333–349.
- Nezlin, N.P., Afanas'yer, Y.D., Ginzburg, A.I., Kostianoy, A.G., 2002. *Adv. Space Res.* 29 (1), 99–106.
- Oguz, T., Gilbert, D., 2006. Abrupt transitions of the top-down controlled Black Sea pelagic ecosystem during 1960–2000: evidence for regime-shifts under strong fishery exploitation and nutrient enrichment modulated by climate-induced variations. *Deep Sea Res. Part I* 54 (2), 220–242.
- Oguz, T., Velikova, V., 2010. Abrupt transition of the northwestern Black Sea shelf ecosystem from a euphotic to an alternative pristine state. *Mar. Ecol. Prog. Ser.* 405, 231–242.
- Oguz, T., Malanotte-Rizzoli, P., Ducklow, H.W., 2001. Simulations of phytoplankton seasonal cycle with multi-level and multi-layer physical-ecosystem models: the Black Sea example. *Ecol. Model.* 144, 295–314.
- Oguz, T., Cokacar, T., Malanotte-Rizzoli, P., Ducklow, H.W., 2003. Climatic warming and accompanying changes in the ecological regime of the Black Sea during 1990s. *Glob. Biogeochem. Cycles* 17 (3), 1088. <http://dx.doi.org/10.1029/2003GB002031>.
- Oguz, T., Tugrul, S., Kideys, A.E., Ediger, V., Kubilay, N., 2005. Physical and biogeochemical characteristics of the Black Sea. *The Sea* 14, 1331–1369 (Chapter 33).
- Oguz, T., Fach, B., Salihoglu, B., 2008. A coupled plankton–anchovy population dynamics model assessing nonlinear controls of anchovy and gelatinous biomass in the Black Sea. *Mar. Ecol. Prog. Ser.* 369, 229–256.
- Ozsoy, E., Unluata, U., 1997. Oceanography of the Black Sea: a review of some recent results. *Earth Sci. Rev.* 42, 231–272.
- Ozsoy, E., Oguz, T., Latif, M.A., Unluata, U., 1986. Oceanography of the Turkish Straits — 1st annual report. Vol. I. Physical oceanography of the Turkish Straits. *Inst. Mar. Sci. METU, Erdemli, Icel*, p. 223.
- Ozsoy, E., Oguz, T., Latif, M.A., Unluata, U., Sur, H.I., Besiktepe, S., 1988. Oceanography of the Turkish Straits — 2nd annual report. Vol. I. Physical oceanography of the Turkish Straits. *Inst. Mar. Sci. METU, Erdemli, Icel*.
- Pauly, D., Christensen, V., Dalsgaard, J., Froese, R., Torres Jr., F., 1998. Fishing down marine food webs. *Science* 279, 860–863.
- Penduff, T., Juza, M., Brodeau, L., Smith, G.C., Barnier, B., Molines, J.M., Treguier, A.M., Madec, G., 2010. Impact of global ocean model resolution on sea-level variability with emphasis on interannual time scales. *Ocean Sci.* 6, 269–284.
- Randall, D.A., Wood, R.A., Boney, S., Coleman, R., Fichet, T., Fyfe, J., Kattsov, V., Pitman, A., Shukla, J., Srinivasan, J., Stouffer, R.J., Sumi, A., Taylor, K.E., 2007. Climate models and their evaluation. In: Solomon, S., Qin, D., Manning, M., Chen, Z., Marquis, M., Averyt, K.B., Tignor, M., Miller, H.L. (Eds.), *Climate Change 2007: The Physical Science Basis. Contribution of Working Group I to the Fourth Assessment Report of the Intergovernmental Panel on Climate Change*. Cambridge University Press, Cambridge, United Kingdom and New York, NY, USA.
- Saux Picart, S., Butenschon, M., Shutler, J.D., 2011. Wavelet-based spatial comparison technique for analysing and evaluating two-dimensional geophysical model fields. *Geosci. Model Dis.* 4, 3161–3182.
- Shiganova, T.A., 1998. Invasion of the Black Sea by the ctenophore *Mnemiopsis leidyi* and recent changes in pelagic community structure. *Fish. Oceanogr.* 7, 305–310.
- Shutler, J.D., Smyth, T.J., Saux-Picart, S., Wakelin, S.L., Hyder, P., Orekhov, P., Grant, M.G., Tilstone, G.H., Allen, J.L., 2011. Evaluating the ability of a hydrodynamic ecosystem model to capture inter- and intra-annual spatial characteristics of chlorophyll-a in the north east Atlantic. *J. Mar. Syst.* 88 (2), 169–182.
- Simpson, J.H., Bowers, D., 1981. Models of stratification and frontal movement in shelf-seas. *Deep-Sea Res.* 28A (7), 727–738.
- Stanev, E.V., 1990. On the mechanisms of the Black Sea circulation. *Earth-Sci. Rev.* 28, 285–319.
- Stanev, E.V., Bowman, M.J., Peneva, E.I., Staneva, J.V., 2003. Control of Black Sea intermediate water mass formation by dynamics and topography: comparison of numerical simulations, surveys and satellite data. *J. Mar. Res.* 61, 59–99.
- Studenikina, E.I., Volovik, S.P., Miryozan, I.A., Luts, G.I., 1991. The ctenophore *Mnemiopsis leidyi* in the Sea of Azov. *Oceanology* 3, 722–725.
- Tugrul, S., Salihoglu, I., 2003. Spatial and temporal variations in the hydrochemical properties of the Black sea upper layer. In: Yilmaz, A. (Ed.), *Oceanography of the Eastern Mediterranean and Black Sea: Similarities and Differences of Two Interconnected Basins*. Tubitak Publishers, Ankara, Turkey.
- Uppala, S.M., Källberg, P.W., Simmons, A.J., Andrae, U., da Costa Bechtold, V., Fiorino, M., Gibson, J.K., Haseler, J., Hernandez, A., Kelly, G.A., Li, X., Onogi, K., Saarinen, S., Sokka, N., Allan, R.P., Andersson, E., Arpe, K., Balmaseda, M.A., Beljaars, A.C.M., van de Berg, L., Bidlot, J., Bormann, N., Caires, S., Chevallier, F., Dethof, A., Dragosavac, M., Fisher, M., Fuentes, M., Hagemann, S., Hólm, E., Hoskins, B.J., Isaksen, I., Janssen, P.A.E.M., Jenne, R., McNally, A.P., Mahfouf, J.-F., Morcrette, J.-J., Rayner, N.A., Saunders, R.W., Simon, P., Sterl, A., Trenberth, K.E., Untch, A., Vasiljevic, D., Viterbo, P., Woollen, J., 2005. The ERA-40 re-analysis. *Quart. J. R. Meteorol. Soc.* 131, 2961–3012. <http://dx.doi.org/10.1256/qj.04.176>.
- Vantrepotte, V., Melin, F., 2009. Temporal variability of 10-year global SeaWiFS time-series of phytoplankton chlorophyll a concentration. *ICES J. Mar. Sci.* 66, 1547–1556.
- Vinogradov, M.E., Shushkina, E.I., Musaeva, E.I., Sorokin, P.Y., 1989. Ctenophore *Mnemiopsis leidyi* (A. Agassiz) (Ctenophora: *Lobata*) — new settler in the Black Sea. *Oceanology* 29, 293–298.
- Vinogradov, M.E., Shushkina, E.A., Anokhina, L., Vostokov, S.V., Kucheruk, N.V., Lukashova, T.A., 2000. Mass development of the ctenophore *Beroe ovata* near the northeastern coast of the Black Sea. *Oceanology* 52–55 (Eng. Transl.).
- Wilby, R.L., Fowler, H.J., 2010. Regional climate downscaling. In: Fung, C.F., Lopez, A., New, M. (Eds.), *Modelling the Impact of Climate Change on Water Resources*. Wiley-Blackwell, Chichester, U.K., pp. 34–85.